Article

Immunity

Brain Endothelial- and Epithelial-Specific Interferon Receptor Chain 1 Drives Virus-Induced Sickness Behavior and Cognitive Impairment

Graphical Abstract

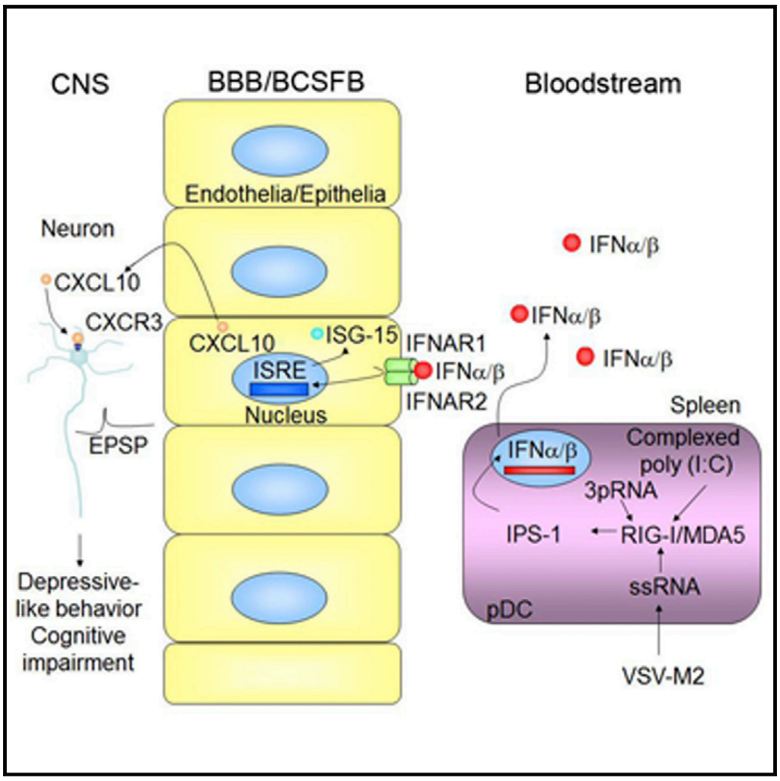

Authors

Thomas Blank, Claudia N. Detje, Alena Spieß, ..., Mathias Heikenwalder, Ulrich Kalinke, Marco Prinz

Correspondence

marco.prinz@uniklinik-freiburg.de

In Brief

Sickness behavior and cognitive dysfunction occur frequently during RNA virus infection by unknown mechanisms. Prinz and colleagues show that virus-induced sickness behavior is induced by interferon receptor chain 1 (IFNAR1) engagement on brain endothelial and epithelial cells that in turn influence neuronal signaling to drive cognitive impairment and depression-like behavior.

Highlights

- Viruses induce depressive behavior and ISG15 expression at the blood-brain barrier
- IFNAR1 expression on neural cells is not involved in IFN-β-induced sickness behavior
- IFNAR1 expression on brain endothelial and epithelial cells drives behavioral changes
- Brain endothelia- and epithelia-derived CXCL10 inhibits hippocampal synaptic plasticity

Accession Numbers

GSE74063

Blank et al., 2016, Immunity *44*, 901–912
April 19, 2016
http://dx.doi.org/10.1016/j.immuni.2016.04.005

Immunity
Article

Brain Endothelial- and Epithelial-Specific Interferon Receptor Chain 1 Drives Virus-Induced Sickness Behavior and Cognitive Impairment

Thomas Blank,[1] Claudia N. Detje,[2] Alena Spieß,[1] Nora Hagemeyer,[1] Stefanie M. Brendecke,[1] Jakob Wolfart,[3] Ori Staszewski,[1] Tanja Zöller,[1] Ismini Papageorgiou,[4] Justus Schneider,[4] Ricardo Paricio-Montesinos,[1] Ulrich L.M. Eisel,[5] Denise Manahan-Vaughan,[6] Stephan Jansen,[6] Stefan Lienenklaus,[2,7] Bao Lu,[8] Yumiko Imai,[9] Marcus Müller,[10] Susan E. Goelz,[11] Darren P. Baker,[12] Markus Schwaninger,[13] Oliver Kann,[4] Mathias Heikenwalder,[14,15] Ulrich Kalinke,[2] and Marco Prinz[1,16,*]

[1]Institute of Neuropathology, University of Freiburg, 79106 Freiburg, Germany
[2]Institute for Experimental Infection Research, TWINCORE, Centre for Experimental and Clinical Infection Research, a joint venture between the Helmholtz Centre for Infection Research and the Medical School Hannover, 30625 Hannover, Germany
[3]Oscar Langendorff Institute of Physiology, University of Rostock, 18057 Rostock, Germany
[4]Institute of Physiology and Pathophysiology, University of Heidelberg, 69120 Heidelberg, Germany
[5]Department of Molecular Neurobiology, Groningen Institute of Evolutionary Life Sciences, University of Groningen, and Department of Psychiatry, University Medical Center Groningen, 9700 Groningen, The Netherlands
[6]Ruhr University Bochum, Medical Faculty, Department Neurophysiology, 44780 Bochum, Germany
[7]Institute for Laboratory Animal Science, Hannover Medical School, Carl-Neuberg-Strasse 1, 30625 Hannover, Germany
[8]Children's Hospital, Harvard Medical School, Boston, MA 02115, USA
[9]Department of Biological Informatics and Experimental Therapeutics, Akita University Graduate School of Medicine, Akita 010-8543, Japan
[10]Department of Neurology, Universitätsklinikum Bonn, 53105 Bonn, Germany
[11]Portland, Oregon, 97201, USA
[12]Biogen Inc., Cambridge, MA 02142, USA
[13]Institute of Experimental and Clinical Pharmacology and Toxicology, University of Lübeck, 23538 Lübeck, Germany
[14]Institute of Virology, Technische Universität München/ Helmholtz-Zentrum München, 81756 München, Germany
[15]Division of Chronic Inflammation and Cancer, German Cancer Research Center (DKFZ), 69120 Heidelberg, Germany
[16]BIOSS Centre for Biological Signalling Studies, University of Freiburg, 79104 Freiburg, Germany
*Correspondence: marco.prinz@uniklinik-freiburg.de
http://dx.doi.org/10.1016/j.immuni.2016.04.005

SUMMARY

Sickness behavior and cognitive dysfunction occur frequently by unknown mechanisms in virus-infected individuals with malignancies treated with type I interferons (IFNs) and in patients with autoimmune disorders. We found that during sickness behavior, single-stranded RNA viruses, double-stranded RNA ligands, and IFNs shared pathways involving engagement of melanoma differentiation-associated protein 5 (MDA5), retinoic acid-inducible gene 1 (RIG-I), and mitochondrial antiviral signaling protein (MAVS), and subsequently induced IFN responses specifically in brain endothelia and epithelia of mice. Behavioral alterations were specifically dependent on brain endothelial and epithelial IFN receptor chain 1 (IFNAR). Using gene profiling, we identified that the endothelia-derived chemokine ligand CXCL10 mediated behavioral changes through impairment of synaptic plasticity. These results identified brain endothelial and epithelial cells as natural gatekeepers for virus-induced sickness behavior, demonstrated tissue specific IFNAR engagement, and established the CXCL10-CXCR3 axis as target for the treatment of behavioral changes during virus infection and type I IFN therapy.

INTRODUCTION

There is a large amount of literature describing the impact of psychological states such as stress, anxiety, and depression on the immune system. In addition, a substantial number of articles have been published indicating that the immune system, in turn, can affect psychological and cognitive function (Allison and Ditor, 2014). However, the underlying signaling pathways and cell types involved are less well known. The observation that common symptoms of viral infections frequently include mood changes such as depressive-like behavior, cognitive deficits, somnolence, headache, and general feeling of malaise (Cunningham et al., 2007) may provide an entrée into studying this link between the immune system and behavior. Viruses that are known to induce behavioral changes (or "viral sickness behavior") as part of the acute phase response include single-stranded (ss)RNA viruses such as influenza or double-stranded (ds)RNA enteroviruses (Dantzer, 2001). Similarly, vesicular stomatitis virus (a ssRNA virus) can induce symptoms of viral sickness behavior in affected individuals (Machida et al., 2013). Type I interferons (IFNs), such as IFN-α and IFN-β, are used in humans for the treatment of malignancies such as hairy cell leukemia, T cell lymphoma of the skin, malignant melanoma, hepatitis C

virus infection (HCV), and multiple sclerosis (Bekisz et al., 2013). In addition to their therapeutic effects, type I IFNs can cause a number of side effects in patients, including symptoms associated with depression such as fatigue, insomnia, irritability, loss of appetite, as well as cognitive changes (Leuschen et al., 2004). Despite its clinical importance, the mechanisms underlying type I IFN-induced depression and cognitive impairment have not been rigorously characterized in research studies.

All viruses produce dsRNA during replication, regardless of the form of nucleic acid carried by the virion (Majde, 2000). dsRNA associated with ssRNA viruses, such as influenza, is thought to be derived primarily from annealing of ssRNA intermediates (Majde, 2000). There are several pattern-recognition receptors implicated in recognition of viral nucleic acids including the membrane bound Toll-like receptors (TLRs), the cytoplasmic helicases RIG-I (retinoic acid-inducible gene I), and the melanoma differentiation-associated gene 5 (MDA5) (Pichlmair and Reis e Sousa, 2007). RIG-I controls innate immune responses to a wide range of RNA viruses, including influenza and vesicular stomatitis virus, whereas MDA5 controls responses to certain picorna viruses (Pichlmair and Reis e Sousa, 2007). dsRNA carrying a 5′-triphosphate (3pRNA) has been identified as the natural ligand for RIG-I and serves as a selective trigger for RIG-I signaling (Hornung et al., 2006). In contrast, the natural ligand for MDA5 is less well-defined, but there is evidence for the involvement of higher order RNA structures and polyinosinic-polycytidylic acid (poly(I:C)), an artificial dsRNA, in MDA5 activation (Kato et al., 2006). MDA5 activation by complexed poly(I:C) requires cytoplasmic delivery (for example, with polyethylenimine (PEI) derivates), whereas non-complexed poly(I:C) activates endosomal TLR3 signaling that induces high levels of proinflammatory cytokines such as interleukin-6 (IL-6) (Kato et al., 2006). Upon receptor engagement by the respective ligands, RIG-I or MDA5 interact with the adaptor protein interferon-β promoter stimulator 1 (IPS-1), also known as mitochondrial antiviral signaling protein (MAVS), to activate downstream signaling cascades that lead to the production of IFNs that counteract the pro-inflammatory cytokines. Similar to IFNs, synthetic dsRNA or virus-derived dsRNA also stimulate sickness behavior indistinguishable from that of influenza virus infection (Kimura-Takeuchi et al., 1992), suggesting similar pathophysiological mechanisms leading to the clinical phenotype. Still, the principal molecular basis and cellular components involved in this disorder have not been explored in detail. In this study, we found that in vivo synthetic dsRNAs, a prototype RNA virus, and recombinant type I IFN, all shared the ability to induce cognitive impairment and mood changes. Peripheral IFN-β activated interferon receptor chain 1 (IFNAR) expressed on brain endothelia and epithelia, which released the cytokine CXCL10 into the brain parenchyma where neuronal function was compromised.

RESULTS

RNA Viruses-Induced Depression Shows ISG15 Expression in Brain Endothelial and Epithelial Cells

To investigate the behavioral changes associated with systemic ssRNA virus infection, we carried out a forced swim test (FST) in mice challenged with the vesicular stomatitis virus (VSV)-M2. Exposed mice showed a depressive-like behavior (Figure 1A) with significantly higher immobility times compared to controls. These behavioral differences were transient and present 24 hr post-infection (hours post-infection, hpi) but were absent 8 weeks post-infection (weeks post-infection, wpi). VSV-M2-associated behavioral changes were unlikely to have been induced by direct viral infection of the central nervous system (CNS) as shown by an absent viable virus titer (Figure 1B).

We then carried out immunohistochemical examination of IFN-stimulated gene (ISG)15 expression in brain sections of infected mice (Figure 1C; Figure S1C). The ISG15 signal was detectable in brain endothelial cells (including capillaries, arterioles, arteries, and venules) of different regions, such as cortex and hippocampus as well as in the meninges, ependymal cells and epithelial cells of the choroid plexus 24 hpi (Figures S2D and S2E), whereas no other CNS cells such as neurons or glial cells expressed it.

We next assessed endogenous type I IFN using a bioluminescence method that takes advantage of an IFN-β reporter system (Lienenklaus et al., 2009). We found a strong tissue-specific induction of IFN-β following infection with VSV-M2, which was restricted to secondary lymphoid organs with no significant signal from brain tissue (Figure 1D). Similar data were obtained using an ELISA-based approach after infection (Figure S3A). To determine the contribution of plasmacytoid dendritic cells (pDCs) to the observed sickness behavior, we treated mice with a pDC-depleting antibody. pDC depletion resulted in a robust protection from virus-induced depressive-like behavior (Figures 1E and 1F). Together, these data indicated that cytokine production by pDCs or alternatively the presence of DCs activated brain endothelia and epithelia and was essential for VSV-M2-evoked sickness behavior.

MAVS Modulates RNA Virus Ligand-Induced Behavior and Cognitive Impairment

VSV-M2 is recognized by cytosolic RIG-I (Jensen and Thomsen, 2012). Notably, 5′-triphosphate RNA molecules derived from either viral RNA or from the synthetically produced 3pRNA can also induce RIG-I activation (Dann et al., 2012), whereas MDA5 stimulation is achieved using complexed poly(I:C), a synthetic analog of viral dsRNA (Dann et al., 2012). To test whether the RIG-I and MDA5 ligands 3pRNA and poly(I:C) can be used in their complexed structures to decipher RNA virus-induced sickness behavior in vivo, we first compared the tissue-specific signaling pathways after systemic challenge with VSV-M2 and the RIG-I and MDA5 ligands and found that type I IFN-regulated pathways were shared by all experimental groups (Figures 2A and 2B).

To determine whether RNA virus-induced depression-like mood changes are dependent on the adaptor MAVS, we challenged mice lacking MAVS with 3pRNA or poly(I:C) in their complexed structures (Figure 2C). Similar to wild-type mice challenged with VSV-M2 (Figure 1A), the RIG-I and MDA5 ligands robustly prolonged the immobility time in the FST. Furthermore, 3pRNA- and poly(I:C)-evoked depressive-like behavior was dependent on the presence of MAVS (Figure 2C). Likewise, ligand-induced impairment of spatial learning in the Morris water maze (MWM) test was rescued in mice lacking MAVS, whereas motoric abilities were not altered (Figure 2D). Impairment of memory induced by RIG-I and MDA5 agonists was found to

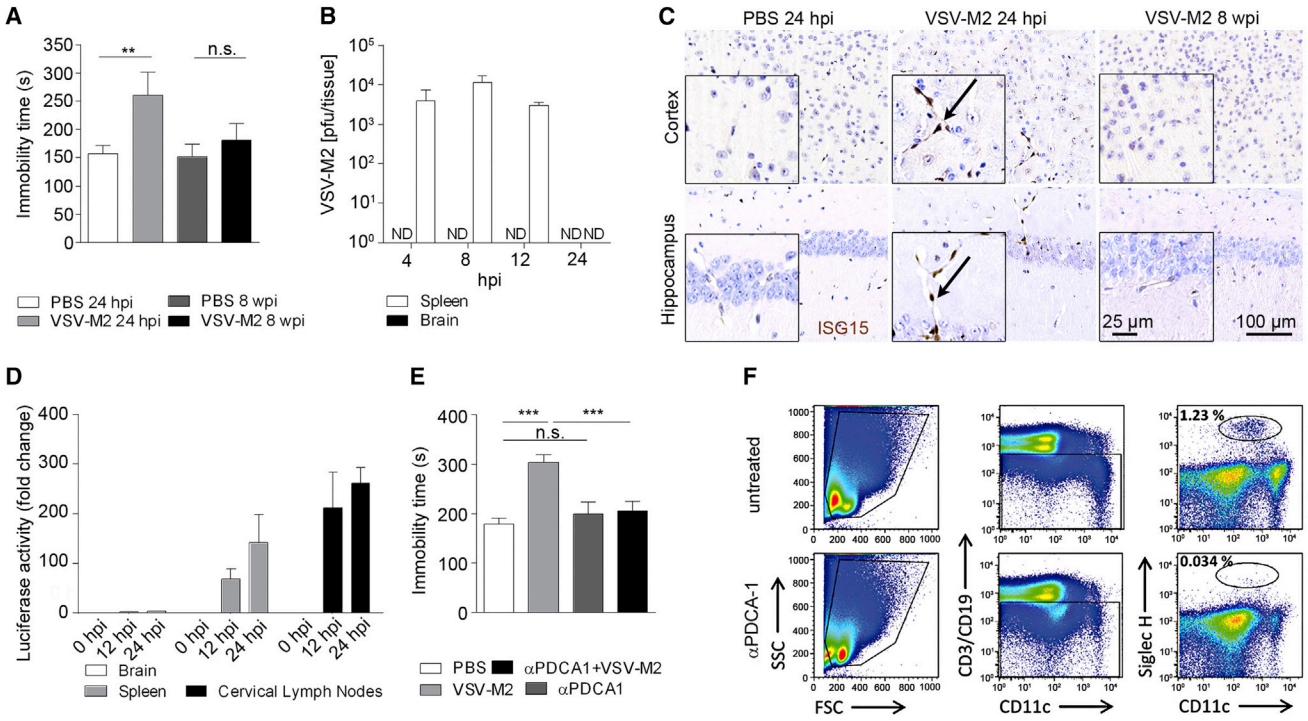

Figure 1. RNA-Virus-Induced Acute Depressive-like Behavior Is Accompanied by Peripheral IFN-β Induction and an IFN Response in Brain Endothelia

(A) Wild-type mice were infected intravenously (i.v.) with VSV-M2 or mock infected with PBS and subjected to the forced swim test 24 hr post-inoculation (hpi) (Mann-Whitney *U* test, p = 0.0081; number of VSV-M2-treated mice, n = 5; number of PBS-treated control mice, n = 8, will be written in the following style n = 5,8) and 8 weeks post-inoculation (wpi) (Mann-Whitney *U* test, n = 5,7). One representative experiment of two is shown. (**p < 0.01, n.s., not significant).

(B) Virus load in brain and spleen of VSV-M2 i.v. infected mice. Tissue was homogenized and the viable virus titer determined using Vero cells. One of three experiments is shown. (n = 5; N.D., not detectable).

(C) Immunohistochemical visualization of the interferon stimulated gene (ISG) 15 in brain endothelial cells after PBS or VSV-M2 exposure. Regions shown are cortex (upper panel) and hippocampus (lower panel) with positive signals marked with arrows. Data are representative of two experiments with six mice each. Scale bars represent 100 μm and 25 μm (inset).

(D) Ex vivo luciferase measurements in tissues of Luc-Cre*Ifnb*$^{fl/fl}$ mice upon i.v. challenge with VSV-M2 normalized to vehicle-treated mice. Bars represent means ± SEM with at least three tissue samples per time point in each group. One representative experiment of two is shown.

(E) Immobility of mice during a FST 24 hpi with PBS (n = 11), an antibody that recognizes the mouse plasmacytoid dendritic cell antigen-1 (αPDCA-1) (n = 6), VSV-M2 (n = 5) or αPDCA-1+ VSV-M2 (n = 6) treatment. One representative experiment of two is shown. (***p < 0.001, n.s., not significant).

(F) Representative dot plots illustrating gating strategy for splenocytes from untreated or pDC-depleted mice 24 hr after αPDCA-1 treatment. Viable cells were gated by forward (FSC) and side scatter (SSC), and CD3$^-$CD19$^-$ cells were analyzed for CD11c$^+$SiglecH$^+$ double positive pDCs. One representative experiment of two is shown. See also Figures S1, S2D, S2E, and S3A.

depend on the presence of MAVS (Figure 2E), whereas visual abilities remained unaltered by treatment (Figure 2F). Accordingly, the IFN response in hippocampal endothelial cells, as visualized by ISG15 immunohistochemistry, was abolished in *Mavs* $^{-/-}$ mice treated with RIG-I or MDA5 ligands (Figure 2G; Figure S1).

We next examined whether recombinant mouse IFN-β might evoke similar behavioral and cognitive changes by utilizing the same pathways. *Mavs*$^{-/-}$ mice were challenged with recombinant IFN-β that was able to significantly increase the immobility in the FST (Figure 2H) but, in contrast to the RIG-I and MDA5 ligands (Figure 2C), the induction of depressive-like behavior was independent from the presence of MAVS (Figure 2H). Similarly, spatial learning in the MWM test was strongly reduced in the presence of recombinant mouse IFN-β and, likewise, did not require MAVS (Figure 2I). Finally, IFN-β treatment significantly decreased memory recall that was not rescued in mice lacking MAVS (Figure 2J), whereas the latency to find the visible platform was not influenced (Figure 2K). In line with these observations, IFN-β induced a detectable interferon signal in brain endothelia in both *Mavs*$^{+/+}$ and *Mavs*$^{-/-}$ mice (Figure 2L; Figures S1, S2B, and S2C). These results show that recombinant IFN-β and 3pRNA and poly(I:C) induced major changes in behavior and cognition that were comparable to those observed after VSV-M2 infection. The effects of VSV-M2 infection and of the viral RNA analogs were dependent on the presence of the adaptor molecule MAVS, while effects mediated through recombinant IFN-β did not require this pathway.

IFNAR1 on Neural Cells Is Not Responsible for Sickness-Behavior

To assess the role and function of the type I interferon receptor (IFNAR1) in virus-induced behavioral and cognitive changes, we tested viral analogs in either IFNAR1-competent or deficient

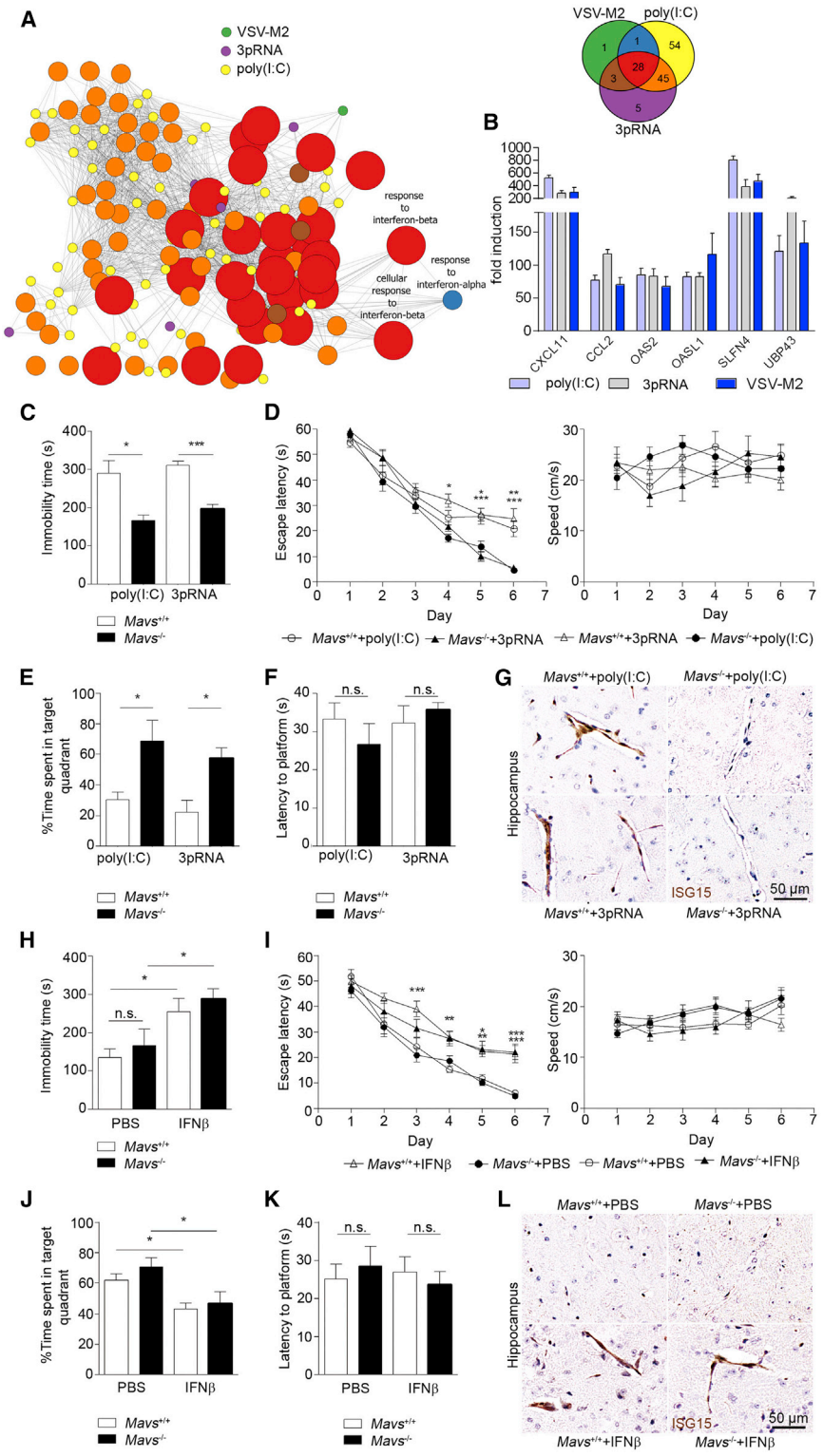

Figure 2. Depressive-like Behavior and Cognitive Impairment Induced by RNA Virus Ligands Are Mediated by MAVS

(A) GO analysis was performed on all significantly differentially regulated genes from splenic cells in mice treated for 24 hr versus control for each of the three conditions shown. Left panel depicts diagram of GO term networks with common interferon pathways labeled. The size of the circles indicates from small to large: size 1, found in one experimental group; size 2, found in two experimental groups; size 3, found in all three experimental groups. Color coding is the same as in the Venn diagram. The Venn diagram (right) shows the number of overlapping GO terms for all significantly differentially regulated genes.

(B) Quantitative RT-PCR of IFN-β-induced genes (selected from the red group of genes in the Venn diagram) in spleens of mice 24 hr after challenge. Data are expressed as the ratio of induced factors normalized to endogenous Gapdh compared to unchallenged controls. One representative experiment of three is shown.

(C) FST of *Mavs*$^{+/+}$ (n = 5,5) and *Mavs*$^{-/-}$ (n = 5,5) mice upon exposure to complexed 3pRNA or complexed poly(I:C) treatment. One representative experiment of two is shown. (*p < 0.05, ***p < 0.001).

(D) Left panel: Morris water maze (MWM) was carried out using mice lacking (*Mavs*$^{-/-}$, n = 5,5) or expressing (*Mavs*$^{+/+}$, n = 5,5) the MDA-5/RIG-I adaptor MAVS. Mice were challenged with complexed 3pRNA or complexed poly(I:C) on days 0, 1, and 2 and trained daily with four trials until day 6. Right panel: Swim speed of all groups on any given training day. One representative experiment of three is shown (*p < 0.05, **p < 0.01, ***p < 0.001).

(E) On day 7 of the MWM, the experimental groups were subjected to a memory test and to (F) a visual platform test. One representative experiment of three is shown. (*p < 0.05; n.s., not significant).

(G) ISG15 immunohistochemistry in hippocampal endothelial cells of *Mavs*$^{-/-}$ mice 24 hpi with complexed 3pRNA or complexed poly(I:C) (n = 6–8).

(H) Immobility measured in the FST in *Mavs*$^{+/+}$ and *Mavs*$^{-/-}$ mice 24 hpi with IFN-β or PBS (n = 5 for each group). One representative dataset of two is shown. (*p < 0.05, n.s., not significant).

(I) Left panel: for MWM *Mavs*$^{+/+}$ and *Mavs*$^{-/-}$ mice were injected daily with either PBS or IFN-β from day 0 to day 6 before learning a water maze task (n = 5 for each group). Right panel: Swim speed upon IFN-β exposure. One representative experiment of three is depicted. (*p < 0.05, **p < 0.01, ***p < 0.001).

(J) On day 7 of MWM, mice were subjected to a memory test. One representative dataset of three is shown. (*p < 0.05).

(K) Visual capacity was determined for all groups. One representative dataset of three is shown. (n.s., not significant).

(L) Visualization of vessel-associated ISG15 in the hippocampi of *Mavs*$^{+/+}$ and *Mavs*$^{-/-}$ mice treated 24 hpi with IFN-β or PBS (n = 7). See also Figures S1, S2A–S2C, S3B, and S4C.

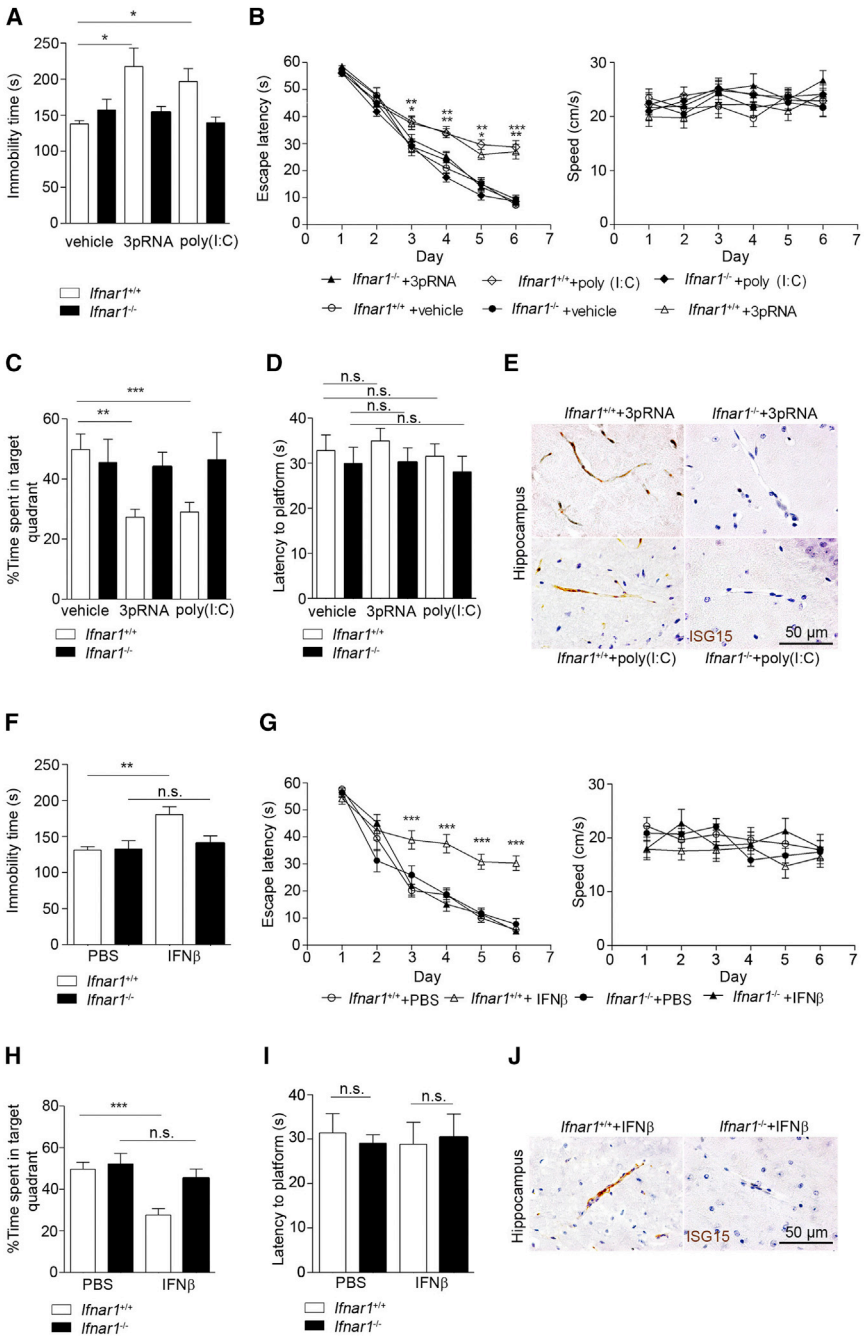

Figure 3. RNA Virus Ligands Elicit Sickness Behavior via IFNAR1

(A) FST with *Ifnar1*$^{+/+}$ and *Ifnar1*$^{-/-}$ mice 24 hpi with vehicle (n = 6,6) or complexed 3pRNA (n = 6,6) or complexed poly(I:C) (n = 7,7). One representative experiment of two is exhibited. (*p < 0.05).

(B) Learning ability in IFNAR1-deficient mice was measured in a MWM test. Mice were injected with complexed 3pRNA or complexed poly(I:C) or vehicle on day 0, 1, and 2, and trained daily with four trials until day 6 (n = 6–7) (left panel). Speed performance in the MWM test of the same groups (right panel). One representative experiment of two is shown. (*p < 0.05, **p < 0.01, ***p < 0.001).

(C) One day after the last training day animals were subjected to the memory test (one representative dataset of two is shown, **p < 0.01, ***p < 0.001) and (D) tested for visual ability in the same experimental groups. One representative result of two is depicted, n.s., not significant.

(E) Chromogenic immunohistochemistry staining for ISG15 in hippocampal sections 24 hr after challenge with complexed 3pRNA or complexed poly(I:C) (n = 7–8).

(F) FST of *Ifnar1*$^{+/+}$ and in *Ifnar1*$^{-/-}$ mice 24 hpi with IFN-β or PBS (n = 6–7). One representative experiment of three is depicted (**p < 0.01).

(G) MWM in *Ifnar1*$^{+/+}$ (n = 7,6) and *Ifnar1*$^{-/-}$ (n = 6,6) mice that were administered with either PBS or IFN-β daily from day 0 to day 6 before learning a water maze task. Right panel: swim speed measurements in all experimental groups over the training period. One representative experiment of three is shown (***p < 0.001).

(H) Quantification of time PBS- and IFN-β-treated mice spent in the target quadrant. (***p < 0.001). One representative experiment of three is shown, n.s., not significant.

(I) Time to find a visible platform was determined in *Ifnar1*$^{-/-}$ or *Ifnar1*$^{+/+}$ mice following the same treatment (n = 6–7). One representative experiment of three is shown, n.s., not significant.

(J) ISG15 expression in hippocampal sections 24 hr following IFN-β administration (n = 7). See also Figures S1, S2, and S5C.

mice (Figure 3A). *Ifnar1*$^{+/+}$ mice developed depressive-like behavior upon RIG-I and MDA5 activation, whereas *Ifnar1*$^{-/-}$ mice were protected from these behavioral changes. In addition, the lack of IFNAR1 was protective for 3pRNA and poly(I:C)-associated impairment of spatial learning (Figure 3B) and memory (Figure 3C), and resulted in the blockade of ISG15 induction in brain endothelial cells (Figure 3E; Figure S1), whereas the latency to find the visible platform was not influenced (Figure 3D). Correspondingly, IFN-β-induced sickness effects were absent in *Ifnar1*$^{-/-}$ mice subjected to the FST (Figure 3F) and the MWM test (Figures 3G–3I), with no detectable ISG15 signals (Figure 3J; Figure S1).

To determine whether IFNAR1 expression on CNS-resident neuroectodermal cells or myeloid cells, including microglia, limits the induction of IFN-linked sickness behavior, we crossed conditional (floxed) IFNAR1 mice with transgenic mouse lines expressing the Cre recombinase under the control of either the nestin or the LysM promoter. As we have shown previously (Prinz et al., 2008), *Ifnar1*$^{fl/fl}$ NesCre mice exhibit a highly efficient IFNAR1 deletion on all neuroectodermal cells (neurons, astrocytes, and oligodendrocytes), whereas *Ifnar1*$^{fl/fl}$ LysMCre mice reveal high IFNAR1 recombination especially in peripheral myeloid cells (Prinz et al., 2008). Upon IFN-β challenge, all *Ifnar1*$^{fl/fl}$ NesCre and *Ifnar1*$^{fl/fl}$ LysMCre mice developed clinical signs of depressive-like behavior in the FST (Figure 4A), impaired learning (Figure 4B) and decreased memory (Figure 4C) in the MWM test, whereas visual ability was not influenced (Figure 4D). In mice of all genotypes, type 1

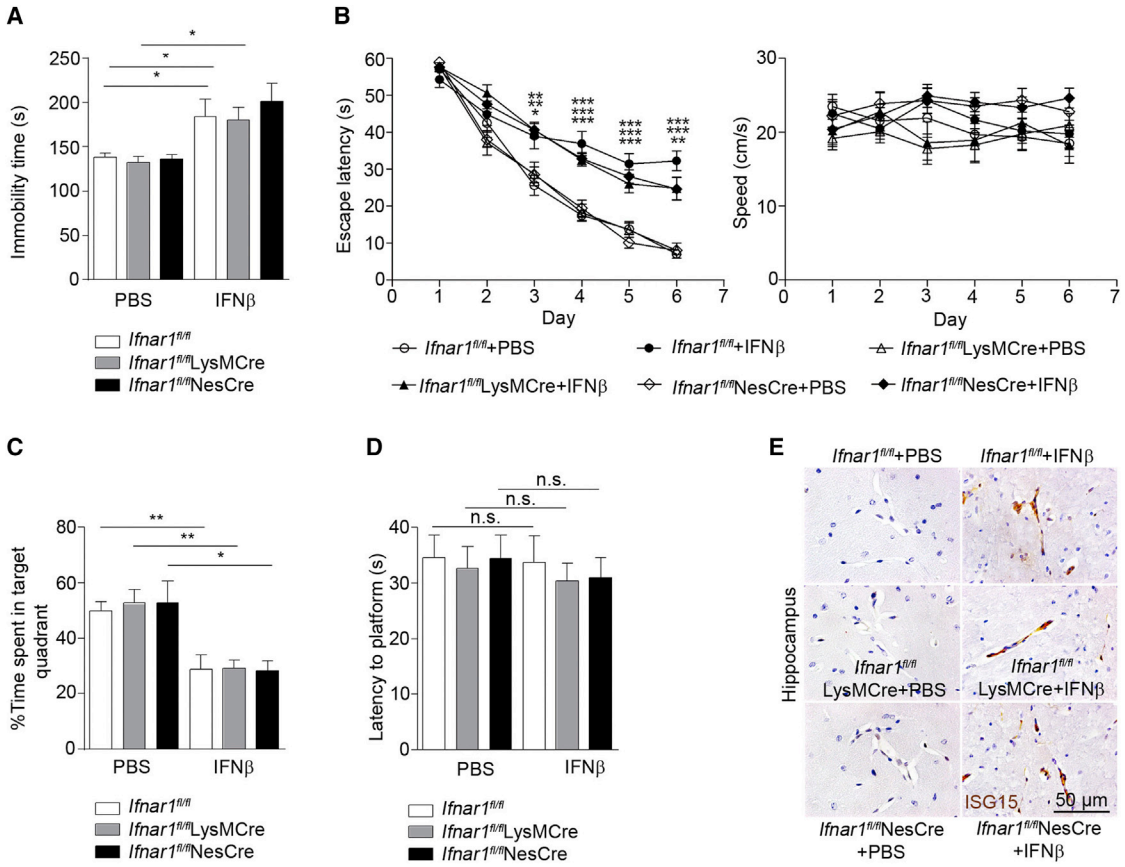

Figure 4. IFNAR1 Expression on Neuroectodermal and Myeloid Cells Is Dispensable for Type I IFN-Evoked Sickness Behavior

(A) FST of *Ifnar1*$^{fl/fl}$ (n = 6,6), *Ifnar1*$^{fl/fl}$ LysMCre (n = 7,6) and *Ifnar1*$^{fl/fl}$ NesCre (n = 7,6) mice 24 hpi of IFN-β or PBS. One representative experiment of two is shown. (*p < 0.05).

(B) Left panel: indicated mouse lines were injected daily with either PBS or IFN-β from day 0 to day 6 while learning a water maze task (n = 6–7). Right panel: Speed measurements during the training period. One representative experiment of two is shown. (*p < 0.05, **p < 0.01, ***p < 0.001).

(C) On day 7 of MWM, mice were subjected to a memory test and to a (D) visual platform test (n = 6–7). One representative experiment of two is shown. (*p < 0.05, **p < 0.01, n.s., not significant).

(E) Immunohistochemistry of ISG15 in hippocampal sections 24 hr following IFN-β or PBS administration (n = 7). See also Figure S1.

IFN induced ISG15 signals in hippocampal endothelia (Figure 4E; Figure S1). These findings were consistent with elevated IFN-β levels observed in the circulation but not locally in the brain after VSV-M2 infection (Figure S3A). Together, these data indicate that IFNAR1 was involved in IFN-β-associated sickness conditions. However, neither neuroectodermal nor myeloid-specific IFNAR1 was an essential modulator of the clinical symptoms.

Non-redundant Functions of Brain Endothelial and Epithelial IFNAR1 for Disease Course

Brain endothelial and epithelial cells are essential parts of the blood-brain barrier (BBB) and the blood-cerebrospinal fluid barrier (BCSFB). As such, they are exposed to proinflammatory mediators as well as danger signals during infections (Dyrna et al., 2013), and therefore might function as decisive cells mediating RNA virus- and IFN-mediated sickness behavior. We first analyzed *Ifnar1*$^{fl/fl}$Slco1c1Cre^{ERT2} mice, which were targeting IFNAR1 specifically on brain endothelial and epithelial cells after injecting tamoxifen, for cell specificity of IFNAR1 deletion (Figure 5A, Figure S4C). Only CD31^{+} brain endothelial cells, but not cells from the heart or lung, showed a strong deletion of *Ifnar1* mRNA four weeks after tamoxifen (TAM) application, indicating high recombination specificity. As a consequence, STAT1 protein phosphorylation was markedly decreased in IFN-β-stimulated brain endothelial cells (Figure 5B). TAM-treated Slco1c1-CreER^{T2}*tdTomato*$^{fl/fl}$ mice, which possess the fluorophore *tdTomato* sitting behind a floxed stop codon in the Rosa26 locus, indicated additional recombination in epithelial cells of the choroid plexus, with no detectable recombination in meninges or ependymal cells (Figure S4C).

We next challenged *Ifnar1*$^{fl/fl}$Slco1c1Cre^{ERT2} mice with IFN-β and measured immobility (Figure 5C) as well as spatial learning and memory capabilities (Figures 5D–5F). Clinical effects were blunted in mice lacking IFNAR1 only on brain endothelial and epithelial cells, whereas speed and visual abilities were not affected. *Ifnar1*$^{fl/fl}$Slco1c1Cre^{ERT2} mice subjected to VSV-M2 were also protected from depressive-like behavior (Figure 5G). Accordingly, the IFN response on endothelia was diminished in *Ifnar1*$^{fl/fl}$Slco1c1Cre^{ERT2} mice upon IFN-β or VSV-M2 administration (Figure 5H; Figure 1). The BBB was still intact following

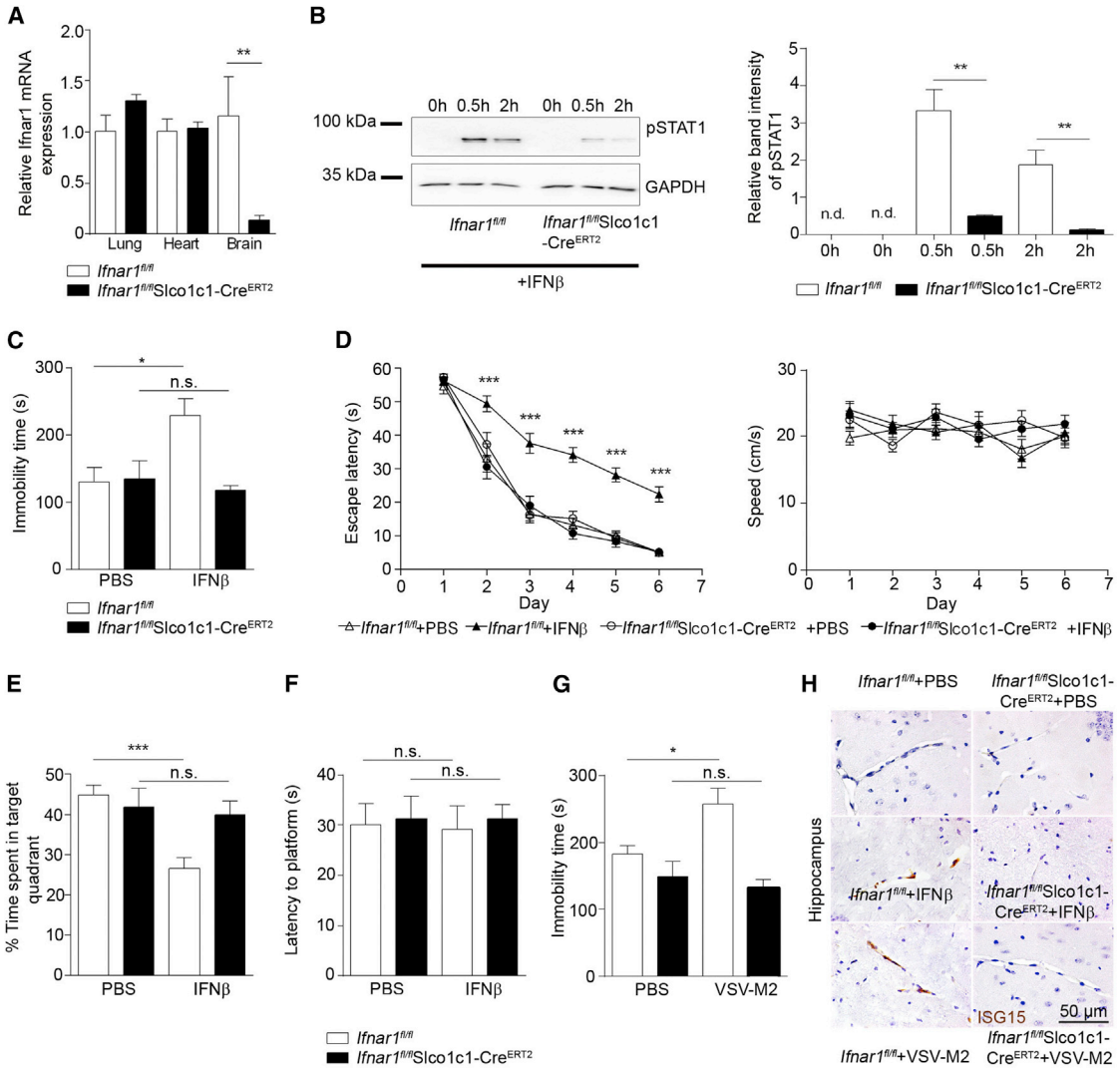

Figure 5. IFNAR1 Signaling by Brain Endothelial Cells Regulates RNA Virus- and IFN-β-Induced Depression and Cognitive Impairment

(A) Deletion of the floxed IFNAR1 locus is shown by quantitative RT-PCR of primary endothelial cells from the lung, heart, and brain of *Ifnar1*$^{fl/fl}$ and *Ifnar1*$^{fl/fl}$Slco1c1-Cre^{ERT2} mice. Data are expressed as the ratio of Ifnar1 mRNA normalized to endogenous Gapdh compared to wild-type levels. One representative experiment of two is shown. (**$p < 0.01$).

(B) Left panel: Immunoblot of STAT1 phosphorylation in primary endothelia challenged with IFN-β revealed reduced in *Ifnar1*$^{fl/fl}$Slco1c1-Cre^{ERT2} mice. Three independent experiments were carried out with one shown. Right panel: pSTAT1 quantification. The pSTAT1 signal is shown in *Ifnar1*$^{fl/fl}$Slco1c1-Cre^{ERT2} mice after 0.5 hr (n = 6) and 2 hr (n = 5) of IFN-β treatment. Error bars represent the mean ± SEM of the intensity measurement of all experiments (*n*) compared to the 0 hr time point and normalized to the endogenous GAPDH level. n.d., not detectable. (**$p < 0.01$).

(C) FST of *Ifnar1*$^{fl/fl}$ and *Ifnar1*$^{fl/fl}$Slco1c1-Cre^{ERT2} mice 24 hpi with either PBS or IFN-β (n = 7 for all groups). One representative experiment out of three is shown. (*$p < 0.05$, n.s., not significant).

(D) MWM test in *Ifnar1*$^{fl/fl}$Slco1c1-Cre^{ERT2} mice compared to *Ifnar1*$^{fl/fl}$ mice (left panel) with normal swim speed in all groups (right panel) (n = 7 for all groups). One representative experiment of three is shown. (***$p < 0.001$).

(E) Memory retention in *Ifnar1*$^{fl/fl}$Slco1c1-Cre^{ERT2} mice compared to *Ifnar1*$^{fl/fl}$ mice. One representative experiment of three is shown. (***$p < 0.001$, n.s., not significant).

(F) Visual abilities were examined measuring the time to reach the visible platform for *Ifnar1*$^{fl/fl}$ and *Ifnar1*$^{fl/fl}$Slco1c1-Cre^{ERT2} mice treated with either PBS or IFN-β. One representative experiment out of three is shown, n.s., not significant.

(G) VSV-M2- and PBS-injected *Ifnar1*$^{fl/fl}$Slco1c1-Cre^{ERT2} and *Ifnar1*$^{fl/fl}$ mice were tested for depressive-like behavior in a FST (n = 7 for all groups). One representative experiment of two is shown. (*$p < 0.05$, n.s., not significant).

(H) ISG15 signals in hippocampal sections obtained from *Ifnar1*$^{fl/fl}$Slco1c1-Cre^{ERT2} mice and *Ifnar1*$^{fl/fl}$ mice 24 hpi with either PBS, VSV-M2 or IFN-β (n = 6). See also Figures S1 and S4C.

treatment as no albumin leakage into the CNS was detectable (Figure 4B), and no reduction of tight junction protein transcripts occurred (Figure 4A). Thus, protection in *Ifnar1*$^{fl/fl}$Slco1c1Cre^{ERT2} mice indicated a vital role of brain endothelia and epithelia for RNA virus-induced changes of cognition and behavior.

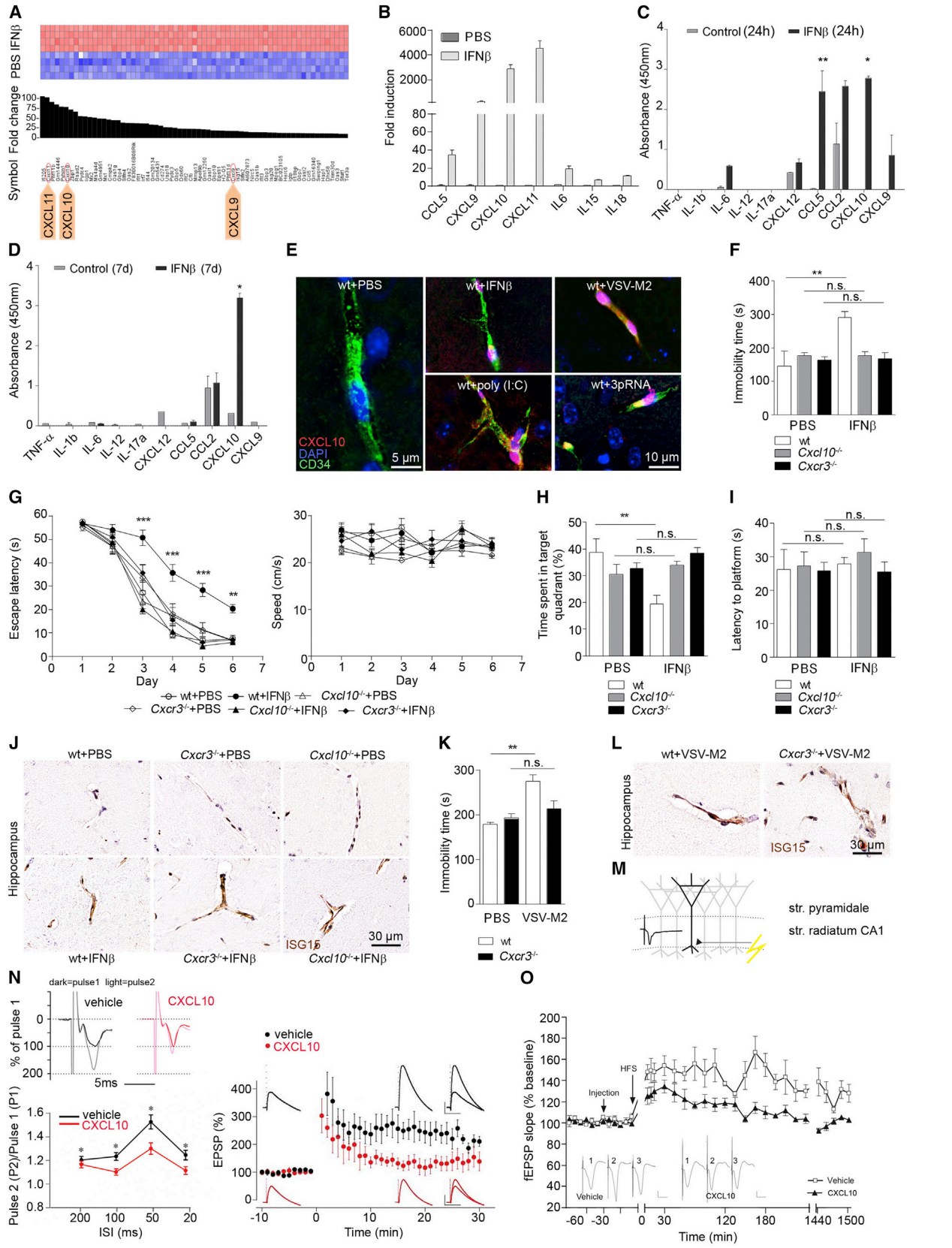

(legend on next page)

CXCL10-CXCR3 Signaling Mediates Sickness Behavior

To better understand how brain endothelial cells modulated IFN-induced sickness behavior, we challenged endothelia with IFN-β and investigated their transcription profile (Figure 6A). The dose of 500 U/mL IFN-β was determined to induce the highest ISG15 expression (Figure S3B). Subsequently, cells were treated for 24 hr with IFN-β and the most significant functional group of genes was found to lie within the chemokine and cytokine module (Figure 6A). Many chemokines, especially CXCL9, CXCL10, and CXCL11, were strongly upregulated, whereas no overt induction of genes indicative of pro-inflammatory responses were detectable, suggesting a primary chemokine-mediated response of brain endothelial cells upon IFN-β challenge. Induction of chemokines was confirmed using qRT-PCR (Figure 6B) and ELISA (Figure 6C) with particularly high release of CXCL10 (Figure 6D). Intra-endothelial production of CXCL10 was evident upon VSV-M2 or virus ligand challenge and after IFN-β incubation (Figure 6E). In response to VSV-M2 infection, elevated CXCL10 protein concentrations were detectable in brain homogenates, in spleen and in blood serum (Figure S3C). CXCR3 as joint receptor for CXCL9, CXCL10, and CXCL11 was found to be expressed in the brain on neurons and microglia (Figure S5A). Mice lacking CXCR3 or CXCL10 subjected to IFN-β treatment were protected from depressive-like behavior (Figure 6F) and impairment of spatial learning and memory (Figures 6G and 6H), whereas the visual system was unaffected (Figure 6I). Endothelial cell induction of ISG15 was independent of the presence of CXCR3 or CXCL10 (Figure 6J; Figure 1). Virus-induced depressive-like changes were absent in *Cxcr3*$^{-/-}$ mice (Figure 6K) despite a strong ISG15 induction in endothelia of brain sections and normal gene expression in brain endothelia from *Cxcr3*$^{-/-}$ mice in response to IFN-β when compared to wild-type (WT) brain endothelia (Figure 6L; Figure S1; Figure S4D). Elevation of CXCL10 in the brain (Figure S3C) did not cause activation of microglia (Figure S5B) nor the recruitment of immune cells to the brain (Figure S6).

We next examined doublecortin (DCX)$^{+}$ cells in the dentate gyrus, where a reduction of DCX^{+} cells can account for cognitive impairment as seen in the MWM and increased depressive-like behavior (Ben Abdallah et al., 2013). However, systemic IFN-β treatment had no effect on the number of DCX^{+} cells (Figure S5C). Next, we examined the synaptic plasticity of adult hippocampal neurons after challenge with CXCL10. Field potentials were recorded in the stratum radiatum of the hippocampal CA1 subregion by stimulation of the fibers between CA3 and CA1 (Figure 6M). Hippocampal slices were incubated with CXCL10 causing reduced paired-pulse facilitation (ratio of second pulse to the first pulse), which is indicative of impaired presynaptic transmitter release (Zucker and Regehr, 2002). The presence of CXCL10 also markedly weakened synaptic long-term potentiation (LTP), an electrophysiological model of learning and memory (Figure 6N). In freely behaving mice, high-frequency afferent stimulation resulted in robust LTP in the hippocampal CA1 region of vehicle-treated animals and persisted for at least 24 hr. Treatment with CXCL10 resulted in a significant impairment of LTP. The impairment obtained after high-frequency stimulation (HFS) was significant throughout the whole recording period, which lasted for 25 hr (Figure 6O).

These data collectively suggest that peripheral challenge with VSV-M2, 3pRNA, or complexed poly(I:C) caused MAVS activation in pDCs and subsequent IFNAR1 activation specifically on brain vessels, followed by an induction of soluble factors such as CXCL10 derived from brain endothelia and epithelia. These soluble factors inhibited short-term- and long-term synaptic

Figure 6. Brain Endothelial IFNAR-CXCL10 Axis Modulates Cognitive Impairment and Sickness Behavior in a CXCR3-Dependent Manner

(A) Affymetrix gene chip array-based heat map (standardized and scaled to $\log_2$ expression) of the 65 most induced transcripts in primary brain endothelia under non-stimulated conditions (PBS) or after IFN-β treatment for 24 hr. The chemokines CXCL9, CXCL10, and CXCL11 are highlighted. One representative experiment of two is shown.

(B) Quantitative RT-PCR in brain endothelial cells after 24 hr of treatment. Data are expressed as the ratio of induced factors normalized to endogenous Gapdh compared to unchallenged controls and show means ± SEM One representative experiment of three is shown.

(C) ELISA-based measurement of cytokine and chemokine secretion in endothelial cell cultures after 24 hr or (D) 7 days of stimulation with IFN-β (500 U/ml). One representative experiment of two is shown. Error bars show means ± SEM with *n* indicating the number of cell cultures from individual mice per group (*$p < 0.05$).

(E) Immunofluorescence for CXCL10 (red) and the endothelial marker CD34 (green). 4',6-diamidino-2-phenylindole (DAPI) in blue. Brain endothelial cells were stimulated for 24 hr with either IFN-β (500 U/ml), complexed poly(I:C), complexed 3pRNA, or PBS. Images of one representative experiment of two are shown.

(F) In a FST, wild-type (WT) (n = 7,5), *Cxcl10*$^{-/-}$ (n = 5,6), and *Cxcr3*$^{-/-}$ (n = 6,6) mice were examined 24 hr after application of IFN-β or PBS. One representative experiment of two is shown (**$p < 0.01$, n.s., not significant).

(G) Left panel: MWM test in WT, *Cxcl10*$^{-/-}$ (n = 5,5), and *Cxcr3*$^{-/-}$ (n = 5,6) mice that were injected daily with either PBS (n = 5,7) or IFN-β from day 0 to day 6 before learning a water maze task. Right panel: Test for swim speed upon PBS and IFN-β injection in the indicated genotypes. One representative experiment of three is shown (**$p < 0.01$, ***$p < 0.001$).

(H) On day 7 of the MWM, mice were subjected to a memory test (one representative experiment out of three is shown, **$p < 0.01$) and the (I) visual capacity was investigated in all three groups. One representative experiment of three is shown. Error bars indicate means ± SEM.

(J) Visualization of ISG15 in hippocampi of *Cxcl10*$^{-/-}$ and *Cxcr3*$^{-/-}$ mice 24 hr after treatment with IFN-β or PBS, (n = 5 for each group).

(K) FST with WT (n = 5,8) and *Cxcr3*$^{-/-}$ (n = 5,5) mice 24 hpi with PBS or VSV-M2. Experiments were carried out twice. One representative result is shown. (**$p <$ 0.01, n.s., not significant).

(L) ISG15 expression in hippocampal tissue of WT and *Cxcr3*$^{-/-}$ mice 24 hpi with VSV-M2. (n = 6).

(M) Scheme of the electrophysiological recordings in the dendritic layer (stratum radiatum) of the hippocampal CA1 subregion following electrical stimulation of the Schaffer collaterals between CA3 and CA1.

(N) Diagram of short-term (left) and long-term potentiation (LTP) (right) with original traces recorded from hippocampal brain slices in the absence (vehicle) or presence of CXCL10 (Wilcoxon signed ranksum test; n = 9,12 slices, n = 7,12 mice).

(O) Effect of intracerebral application of CXCL10 (n = 5, red traces), 30 min prior to high-frequency stimulation (HFS, 100Hz, 50 pulses given 4 times at 5 min intervals) on LTP in freely behaving adult mice compared to vehicle-injected controls (n = 7, black traces). Line-breaks indicate change in time-scale. Insets: representative analogs of fEPSPs recorded in vehicle or CXCL10-treated animals 1) pre-HFS, 2) 5 min post-HFS and 3) 24 hr post-HFS. Horizontal scale bar: 1 mV, vertical scale bar: 10 ms. See also Figures S1, S3C, S4A, S4B, S4D, S5A, S5B, and S6.

plasticity, which positively correlated with the observed behavioral phenotypes.

DISCUSSION

Here we identified the cellular targets and the underlying molecular pathways involved in RNA virus and type I IFN-associated sickness syndrome. We demonstrated that VSV-M2, synthetic dsRNA ligands, as well as IFN-β shared the ability to induce cognitive impairment and behavioral dysfunction by affecting similar cells, and by employing identical molecular switches. We found that the splenic MAVS pathway and its activation by RNA ligands with subsequent stimulation of RIG-I and MDA5 as equivalent to VSV-M2 infection were important for sickness behavior. The presence of IFNs in the circulation stimulated IFNAR1-dependent production of chemokines by brain endothelial and epithelial cells. These chemokines could then mediate fundamental changes in synaptic network function and coupled cognitive functions by engagement of neuronal CXCR3.

Our data also provide evidence that dendritic cells, especially pDCs, are the first and main immunoregulatory cell type that responds to ssRNA infection or exposure to dsRNA ligands that induces a complex cascade of cellular events that lead to sickness behavior and cognitive dysfunction. However, whether pDC-derived type I IFNs or other DC-related functions provide protection from virus-induced sickness behavior remains unclear.

Several studies have found that type I IFNs have several strong effects on the CNS such as synaptic plasticity (Mendoza-Fernández et al., 2000), ingestive behavior (Plata-Salamán, 1992), and emotion (Schrott and Crnic, 1996). There is mounting evidence that the functions of type I IFNs are associated with brain effects in several clinical conditions such as familiar Aicardi-Goutieres syndrome (Prinz and Knobeloch, 2012). In addition, high frequencies of depression, anxiety, and memory loss in patients treated with high doses of type I IFNs have been reported (Leuschen et al., 2004). However, the molecular basis for neuromodulatory actions, especially neuropsychiatric and cognitive complications associated with systemic IFN treatment remains enigmatic. In this study, we identified brain endothelial and epithelial cells as a natural barrier of IFN-mediated sickness behavior. The selective and non-redundant IFNAR1 engagement on endothelial and epithelial cells, especially in the brain but not in peripheral tissues, points to distinct spatial and temporal effects of type I IFNs in the CNS. Although IFNAR1 on meninges or ependymal cells were not targeted by Slco1c1Cre^{ERT2}-deleter mice, sickness behavior was absent in those mice, indicating that brain endothelial and epithelial cells of the choroid plexus are the main source of IFN-induced CXCL10 release. Brain endothelia and epithelia have been shown to be an important mediator of the immune-to-brain communication during IL-1β-induced fever (Ridder et al., 2011).

Upon systemic application of recombinant IFN-α, one study described direct effects on parenchymal CNS cells (e.g., neurons and glia) by rapid induction of IFN-stimulated genes such as STAT1 (Wang et al., 2008). However, in contrast to that report we observed induction of the IFN-stimulated gene ISG15 in brain endothelial and epithelial cells only and not in other CNS cells. IFN-α and IFN-β might target different cell types in the CNS and the periphery with a greater degree of unwanted side effects in the case of IFNα. In addition, depletion of IFNAR1 on neuroectodermal cells including neurons and macroglia by using *Ifnar1*$^{fl/fl}$ NesCre did not protect mice from type 1 IFN-induced sickness. In contrast, only brain endothelial and epithelial- specific IFNAR1 deletion in *Ifnar1*$^{fl/fl}$Slco1c1-Cre^{ERT2} mice provided genetic evidence for this tissue-specific IFNAR1 function. Myeloid specific IFNAR1 deletion that is important for CNS inflammation (Prinz et al., 2008) did not contribute to disease pathogenesis.

Our data on the effects of type I IFNs outside the CNS were also supported by pharmacological studies that estimated that only a small fraction (less than 0.2%) of peripherally-administered IFNs gain access to the CNS (Billiau et al., 1981).

Previously described directs effects of type I IFNs on neurons such as increased inhibitory postsynaptic effects on CA1 pyramidal cells leading to reduced long-term potentiation (Mendoza-Fernández et al., 2000), inhibition of glutamate-induced excitatory postsynaptic potentials of CA3 hippocampal neurons on rodents (Müller et al., 1993), or on the development of neural stem cells (Zheng et al., 2014), do not account for the effects we observed after ssRNA virus infection or dsRNA ligand challenge. In contrast, we identified the chemokines CXCL9, CXCL10, and CXCL11 and their joint receptor CXCR3 as the essential modulator of neuronal plasticity. In our electrophysiological experiments we observed, in accordance with previous findings (Vlkolinský et al., 2004), reduced paired-pulse facilitation and impaired long-term potentiation in the CA1 region of the hippocampus in the presence of CXCL10 in vivo and in vitro. However, our in vitro data showed a more pronounced inhibition of paired-pulse facilitation with effects on all interstimulus intervals investigated when compared to published data (Vlkolinský et al., 2004). Impaired cognitive performance, in correlation with reduced long-term potentiation and short-term plasticity (paired-pulse responses), has been described in depth previously (Lynch, 2004). Paired-pulse responses, as seen in this study, are thought to depend primarily on presynaptic mechanisms including neurotransmitter release (Zucker and Regehr, 2002). Hence, the reduction in paired-pulse facilitation after CXCL10 application pointed to impaired neurotransmitter release, which could also underlie the observed increase in depressive-like behavior. This hypothesis is supported by recent data showing a causal link between the reduction of hippocampal glutamatergic transmission and a depressive-like phenotype in rodents (Marrocco et al., 2014) and patients with major depressive disorder (MDD) (Kohli et al., 2011). In support of our data, patients suffering from MDD show increased peripheral protein concentrations of CXCL10, which are assumed to be similarly elevated in the brain as serum and CSF levels of chemokines appear to correlate (Wong et al., 2008). When we analyzed CXCL10 after VSV-M2 infection, elevated CXCL10 protein levels were not only detected in the brain but also in the spleen and serum. This finding might imply that CXCL10 could also cross the BBB, enter the brain, and subsequently contribute to inhibit neuronal function. Although this possibility cannot be fully excluded, it seems unlikely because the expression of tight junction genes was unaltered during all conditions. Additional evidence was provided by our observation that the BBB tightness, as verified by potential albumin leakage, was not compromised by any treatment. There was also no detectable recruitment of immune cells to the brain parenchyma after VSV-M2 infection, which further indicates an intact BBB. Even if certain

amounts of CXCL10 from the periphery should be able to penetrate the BBB, they could not be the main reason for the observed behavioral changes. This conclusion is based on the fact that deletion of IFNAR from brain endothelia and epithelia prevented IFN-β or VSV-M2-induced sickness behavior. CXCL10 could either bind directly to CXCR3 expressed on neurons, which directly inhibits neuronal plasticity, or first act on microglial CXCR3, to modulate neuronal function in a second step. In that case, microglia would have to be activated as indicated by elevated expression of major histocompatibility complex class II (MHCII) (Benveniste et al., 2001). However, we could not observe upregulation of MHC class II after any of the different treatments. Upon IFN-β challenge endothelial cells in vitro readily released CXCL10 into the medium. But how was CXCL10 reaching its neuronal receptor CXCR3 in situ? Simple diffusion is one explanation because recombinant CXCL10 directly applied to the bath or injected into the mouse brain, elicited changes in synaptic plasticity.

In summary, our study provides evidence for the importance of brain endothelial and epithelial cells in the communication between the CNS and the immune system, and demonstrates tissue specific IFNAR1 engagement during sickness behavior. By the identification of the IFN-induced CXCL10/CXCR3 axis, we offer new drug targets for the management of behavioral impairment during virus infection and type I IFN therapy.

EXPERIMENTAL PROCEDURES

Mice

All animal experiments were approved by the Federal Ministry for Nature, Environment and Consumers' Protection of the states of Baden-Württemberg (35-9185.81/G12/71), Lower Saxony and Mecklenburg-Vorpommern and were carried out in accordance to the respective national, federal, and institutional regulations. Male mice only were used for the experiments. Mice were group housed up to five per cage with 12 hr light/dark cycle with lights on at 6:00 a.m. Food and water were available ad libitum. A detailed description of mice and mouse treatment is given in the Supplemental Experimental Procedures.

Behavioral Testing

The behavioral tests were conducted using male offspring aged 8 to 16 weeks. Mice were first tested in the Morris water maze (MWM), followed 1 day later by the forced swim test (FST). All the water maze and forced swim tests were run between 1 and 5 p.m. (i.e., during the light cycle). In control experiments, an additional cohort of mice was raised in the reversed 12:12 light/dark cycles (lights on at 9:00 p.m.) and tested in the dark phase, under incandescent red light illumination. Data obtained from the two cohorts were strikingly similar (data not shown). Details for the MWM and FST can be found in the Supplemental Experimental Procedures.

Endothelial Cell Culture

Primary mouse brain endothelial cells (PBECs) were prepared from 2 to 6 months old genetically-modified mice that had been injected with tamoxifen (TAM) at the age of 5 to 6 weeks of age as described previously (Ridder et al., 2011). For details see Supplemental Experimental Procedures.

Microarray

Transcriptional profiles of whole spleen tissues and brain endothelial cells were assessed using Affymetrix® Mouse Gene 2.1 ST Array.

ELISA and ELISA Cytokine Assay

Culture media was collected at 7 and 24 hr after IFN-β treatment. The media were immediately concentrated using centrifugal filters (Amicon Ultra, 3K, Millipore) for 30 min at 14,000 g and then stored at −80°C until analysis. The IFN-β levels in the culture media were measured using ELISA cytokine assay kits (SABiosciences) according to the manufacturer's instructions. For CXCL10 (R&D Systems) and High Sensitivity IFN-β ELISA (PBL Assay Science) serum was collected and brain and spleen tissue was homogenized in 1 ml buffer (20 mM Tris/HCl, pH 7.3 with 140 mM NaCl, 0.5% Triton X-100 supplemented with Complete Mini protease inhibitor [Roche] and 2 mM sodium orthovanadate) using Lysing Matrix D (brain) and A (spleen) in a FastPrep homogenator (MP Biomedical). Debris-free supernatant was used and ELISA was performed according to manufacturer's protocol.

VSV-M2 Plaque Assay

After infected tissues were removed at indicated time points and homogenized in 1 ml of medium, serial 10-fold dilutions of homogenates were transferred onto confluent Vero cell (ACC33, Leibniz Institute DSMZ, Germany) monolayers in six-well plates and incubated for 1 hr at 37°C. Monolayers were overlaid with 2 ml of MEM containing 1% methylcellulose and incubated for 24 hr at 37°C. The overlay was then removed, and the monolayer was fixed and stained using 0.5% crystal violet dissolved in 5% formaldehyde, 50% ethanol, and 4.25% NaCl.

Flow Cytometry

To determine the depletion efficiency of αPDCA-1 antibody, we stained splenocytes for CD3 (eBioscience), CD19 (Southern Biotech), CD11c (BD PharMingen), and SiglecH (eBioscience). Cells were washed, fixed with 1% PFA, and analyzed using a LSR II sorb (Becton Dickinson) flow cytometer. Data were acquired with FACSdiva software (Becton Dickinson). Post-acquisition analysis was carried out using FlowJo Software 7.9 (Tree Star).

qRT-PCR

RNA from PBECs and mouse spleen was isolated using the Arcturus Pico kit (Applied Biosystems) or the RNeasy Mini kit (QIAGEN), respectively, according to the manufacturer's protocol. Samples were treated with DNase I (Roche) and 200 ng (PBECs) or 1 μg (spleen) of RNA was transcribed into cDNA using oligo(dT) primers and the SuperScript II RT kit (Invitrogen) or by using the high capacity kit (Applied Biosystems). 1 μl cDNA was transferred into a 96-well Multiply PCR plate (Sarstedt) with 11.5 μl ABsolute QPCR SYBR Green master mix (Thermo Fisher). RT-PCR reactions were carried out as described previously (Dann et al., 2012). A list of primers is provided under Supplemental Experimental Procedures.

Western Blot Analysis

PBECs cells were cultured in 6-well plates. Cells were stimulated with 500 U/mL of mouse IFN-β for the indicated times, lysed in 4× Laemmli buffer containing 400 mM DTT, incubated at 90°C for 10 min, loaded on SDS-PAGE gels, and immunoblotted using antibodies against Gapdh (1:1,000, Mab374, Millipore) and pSTAT (1:1,000, 58D6, Cell Signaling).

For details regarding statistical analysis, see Supplemental Experimental Procedures.

ACCESSION NUMBERS

The datasets of all microarray analyses are deposited at Gene Expression Omnibus (GEO) (GSE74063).

SUPPLEMENTAL INFORMATION

Supplemental Information includes six figures and Supplemental Experimental Procedures and can be found with this article online at http://dx.doi.org/10.1016/j.immuni.2016.04.005.

AUTHOR CONTRIBUTION

T.B., C.N.D., A.S., N.H., S.M.B., J.W., O.K., T.Z., I.P., R.P.-M., D.M.-V., S.J., and J.S. conducted experiments. M.P. and T.B. supervised the project and wrote the manuscript. M.M., M.S., U.K., B.L., S.L., and Y.I. provided genetically modified mice and analyzed the results. D.P.B. and S.E.G. provided mouse IFN-β and analyzed the data. M.H., O.S., and U.L.M.E. designed parts of the project and analyzed the results.

ACKNOWLEDGMENTS

We thank Maria Oberle, Margarethe Ditter, and Christine El Gaz for excellent technical assistance and Silke Dirken for animal care. M.P. was supported by the BMBF-funded competence network of multiple sclerosis (KKNMS), the competence network of neurodegenerative disorders (KNDD), the DFG (PR 577/8-1, Reinhart-Koselleck grant), the ERA-Net NEURON initiative "NEURO-IFN," and the Gemeinnützige Hertie Foundation (GHST). T.B. was supported by the Marie Curie Integration Grant project N° 248033- MBfUSE-DIT submitted under the Call FP7-PEOPLE-2009-RG and the DFG (BL 1153/1-1). D.M.-V. was supported by the SFB 874/B1. U.K. was supported by the Niedersachsen-Research Network on Neuroinfectiology (N-RENNT) of the Ministry of Science and Culture of Lower Saxony, Germany, and the SFB 854 (TP B15 to U.K.) of the German Research Council. Mouse IFN-β was supplied by Biogen Inc. D.P.B. is an employee of Biogen and owns company stock.

Received: November 3, 2014
Revised: October 19, 2015
Accepted: January 5, 2016
Published: April 19, 2016

REFERENCES

Allison, D.J., and Ditor, D.S. (2014). The common inflammatory etiology of depression and cognitive impairment: a therapeutic target. J. Neuroinflammation *11*, 151.

Bekisz, J., Sato, Y., Johnson, C., Husain, S.R., Puri, R.K., and Zoon, K.C. (2013). Immunomodulatory effects of interferons in malignancies. J. Interferon Cytokine Res. *33*, 154–161.

Ben Abdallah, N.M., Filipkowski, R.K., Pruschy, M., Jaholkowski, P., Winkler, J., Kaczmarek, L., and Lipp, H.P. (2013). Impaired long-term memory retention: common denominator for acutely or genetically reduced hippocampal neurogenesis in adult mice. Behav. Brain Res. *252*, 275–286.

Benveniste, E.N., Nguyen, V.T., and O'Keefe, G.M. (2001). Immunological aspects of microglia: relevance to Alzheimer's disease. Neurochem. Int. *39*, 381–391.

Billiau, A., Heremans, H., Ververken, D., van Damme, J., Carton, H., and de Somer, P. (1981). Tissue distribution of human interferons after exogenous administration in rabbits, monkeys, and mice. Arch. Virol. *68*, 19–25.

Cunningham, C., Campion, S., Teeling, J., Felton, L., and Perry, V.H. (2007). The sickness behaviour and CNS inflammatory mediator profile induced by systemic challenge of mice with synthetic double-stranded RNA (poly I:C). Brain Behav. Immun. *21*, 490–502.

Dann, A., Poeck, H., Croxford, A.L., Gaupp, S., Kierdorf, K., Knust, M., Pfeifer, D., Maihoefer, C., Endres, S., Kalinke, U., et al. (2012). Cytosolic RIG-I-like helicases act as negative regulators of sterile inflammation in the CNS. Nat. Neurosci. *15*, 98–106.

Dantzer, R. (2001). Cytokine-induced sickness behavior: mechanisms and implications. Ann. N Y Acad. Sci. *933*, 222–234.

Dyrna, F., Hanske, S., Krueger, M., and Bechmann, I. (2013). The blood-brain barrier. J. Neuroimmune Pharmacol. *8*, 763–773.

Hornung, V., Ellegast, J., Kim, S., Brzózka, K., Jung, A., Kato, H., Poeck, H., Akira, S., Conzelmann, K.K., Schlee, M., et al. (2006). 5′-Triphosphate RNA is the ligand for RIG-I. Science *314*, 994–997.

Jensen, S., and Thomsen, A.R. (2012). Sensing of RNA viruses: a review of innate immune receptors involved in recognizing RNA virus invasion. J. Virol. *86*, 2900–2910.

Kato, H., Takeuchi, O., Sato, S., Yoneyama, M., Yamamoto, M., Matsui, K., Uematsu, S., Jung, A., Kawai, T., Ishii, K.J., et al. (2006). Differential roles of MDA5 and RIG-I helicases in the recognition of RNA viruses. Nature *441*, 101–105.

Kimura-Takeuchi, M., Majde, J.A., Toth, L.A., and Krueger, J.M. (1992). The role of double-stranded RNA in induction of the acute-phase response in an abortive influenza virus infection model. J. Infect. Dis. *166*, 1266–1275.

Kohli, M.A., Lucae, S., Saemann, P.G., Schmidt, M.V., Demirkan, A., Hek, K., Czamara, D., Alexander, M., Salyakina, D., Ripke, S., et al. (2011). The neuronal transporter gene SLC6A15 confers risk to major depression. Neuron *70*, 252–265.

Leuschen, M.P., Filipi, M., and Healey, K. (2004). A randomized open label study of pain medications (naproxen, acetaminophen and ibuprofen) for controlling side effects during initiation of IFN beta-1a therapy and during its ongoing use for relapsing-remitting multiple sclerosis. Mult. Scler. *10*, 636–642.

Lienenklaus, S., Cornitescu, M., Zietara, N., Łyszkiewicz, M., Gekara, N., Jabłónska, J., Edenhofer, F., Rajewsky, K., Bruder, D., Hafner, M., et al. (2009). Novel reporter mouse reveals constitutive and inflammatory expression of IFN-beta in vivo. J. Immunol. *183*, 3229–3236.

Lynch, M.A. (2004). Long-term potentiation and memory. Physiol. Rev. *84*, 87–136.

Machida, M., Ambrozewicz, M.A., Breving, K., Wellman, L.L., Yang, L., Ciavarra, R.P., and Sanford, L.D. (2013). Sleep and behavior during vesicular stomatitis virus induced encephalitis in BALB/cJ and C57BL/6J mice. Brain Behav. Immun. *35*, 125–134.

Majde, J.A. (2000). Viral double-stranded RNA, cytokines, and the flu. J. Interferon Cytokine Res. *20*, 259–272.

Marrocco, J., Reynaert, M.L., Gatta, E., Gabriel, C., Mocaër, E., Di Prisco, S., Merega, E., Pittaluga, A., Nicoletti, F., Maccari, S., et al. (2014). The effects of antidepressant treatment in prenatally stressed rats support the glutamatergic hypothesis of stress-related disorders. J. Neurosci. *34*, 2015–2024.

Mendoza-Fernández, V., Andrew, R.D., and Barajas-López, C. (2000). Interferon-alpha inhibits long-term potentiation and unmasks a long-term depression in the rat hippocampus. Brain Res. *885*, 14–24.

Müller, M., Fontana, A., Zbinden, G., and Gähwiler, B.H. (1993). Effects of interferons and hydrogen peroxide on CA3 pyramidal cells in rat hippocampal slice cultures. Brain Res. *619*, 157–162.

Pichlmair, A., and Reis e Sousa, C. (2007). Innate recognition of viruses. Immunity *27*, 370–383.

Plata-Salamán, C.R. (1992). Interferons and central regulation of feeding. Am. J. Physiol. *263*, R1222–R1227.

Prinz, M., and Knobeloch, K.P. (2012). Type I interferons as ambiguous modulators of chronic inflammation in the central nervous system. Front. Immunol. *3*, 67.

Prinz, M., Schmidt, H., Mildner, A., Knobeloch, K.P., Hanisch, U.K., Raasch, J., Merkler, D., Detje, C., Gutcher, I., Mages, J., et al. (2008). Distinct and nonredundant in vivo functions of IFNAR on myeloid cells limit autoimmunity in the central nervous system. Immunity *28*, 675–686.

Ridder, D.A., Lang, M.F., Salinin, S., Röderer, J.P., Struss, M., Maser-Gluth, C., and Schwaninger, M. (2011). TAK1 in brain endothelial cells mediates fever and lethargy. J. Exp. Med. *208*, 2615–2623.

Schrott, L.M., and Crnic, L.S. (1996). Increased anxiety behaviors in autoimmune mice. Behav. Neurosci. *110*, 492–502.

Vlkolinský, R., Siggins, G.R., Campbell, I.L., and Krucker, T. (2004). Acute exposure to CXC chemokine ligand 10, but not its chronic astroglial production, alters synaptic plasticity in mouse hippocampal slices. J. Neuroimmunol. *150*, 37–47.

Wang, J., Campbell, I.L., and Zhang, H. (2008). Systemic interferon-alpha regulates interferon-stimulated genes in the central nervous system. Mol. Psychiatry *13*, 293–301.

Wong, M.L., Dong, C., Maestre-Mesa, J., and Licinio, J. (2008). Polymorphisms in inflammation-related genes are associated with susceptibility to major depression and antidepressant response. Mol. Psychiatry *13*, 800–812.

Zheng, L.S., Hitoshi, S., Kaneko, N., Takao, K., Miyakawa, T., Tanaka, Y., Xia, H., Kalinke, U., Kudo, K., Kanba, S., et al. (2014). Mechanisms for interferon-α-induced depression and neural stem cell dysfunction. Stem Cell Reports *3*, 73–84.

Zucker, R.S., and Regehr, W.G. (2002). Short-term synaptic plasticity. Annu. Rev. Physiol. *64*, 355–405.

Immunity, Volume *44*

Supplemental Information

Brain Endothelial- and Epithelial-Specific Interferon Receptor Chain 1 Drives Virus-Induced Sickness Behavior and Cognitive Impairment

Thomas Blank, Claudia N. Detje, Alena Spieß, Nora Hagemeyer, Stefanie M. Brendecke, Jakob Wolfart, Ori Staszewski, Tanja Zöller, Ismini Papageorgiou, Justus Schneider, Ricardo Paricio-Montesinos, Ulrich L.M. Eisel, Denise Manahan-Vaughan, Stephan Jansen, Stefan Lienenklaus, Bao Lu, Yumiko Imai, Marcus Müller, Susan E. Goelz, Darren P. Baker, Markus Schwaninger, Oliver Kann, Mathias Heikenwalder, Ulrich Kalinke, and Marco Prinz

Fig. 1C

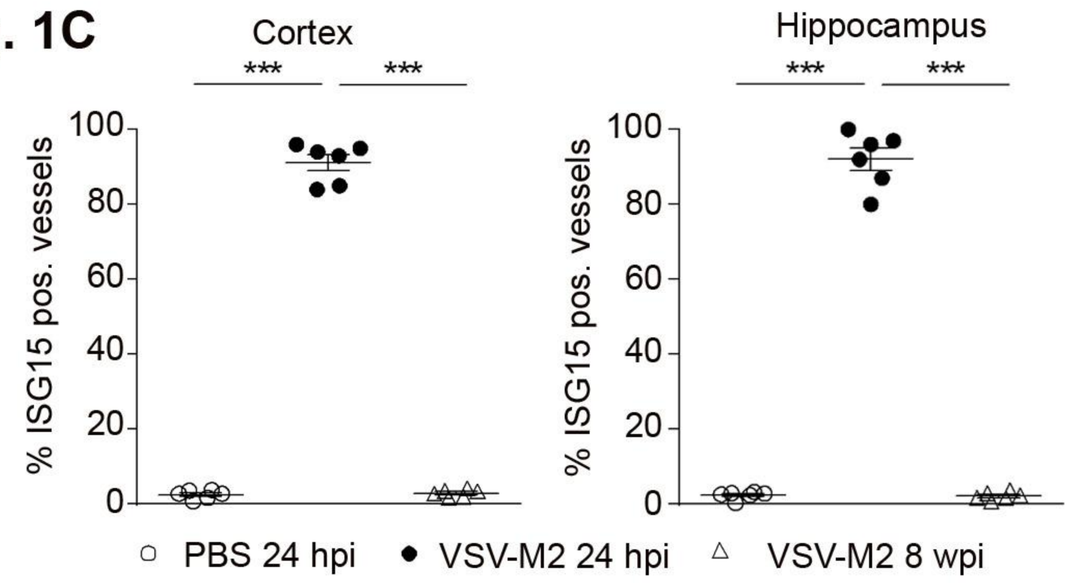

Fig. 2G

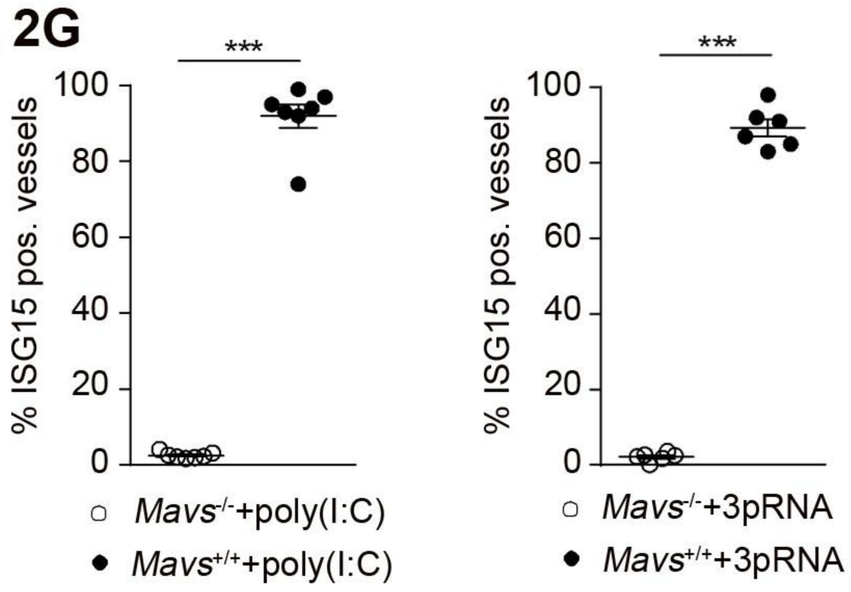

Fig. 2L

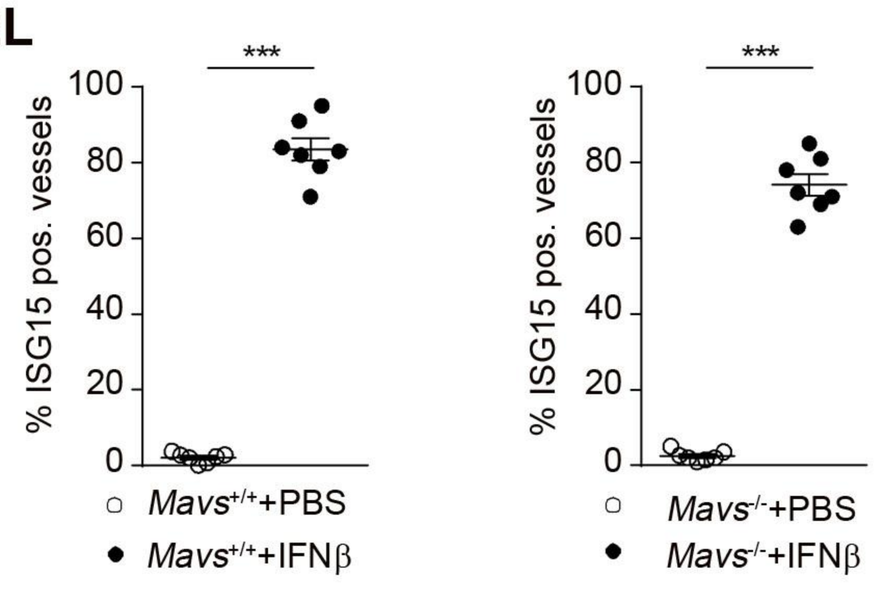

Fig. 3E

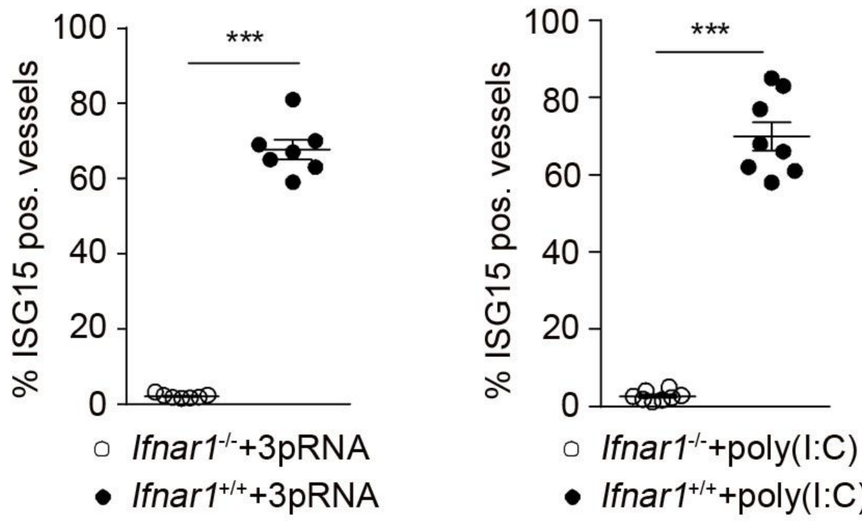

Fig. 3J

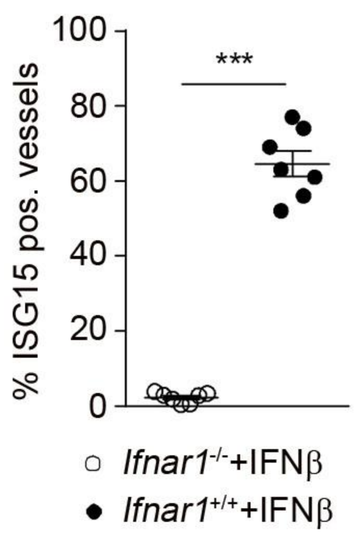

Fig. 3O

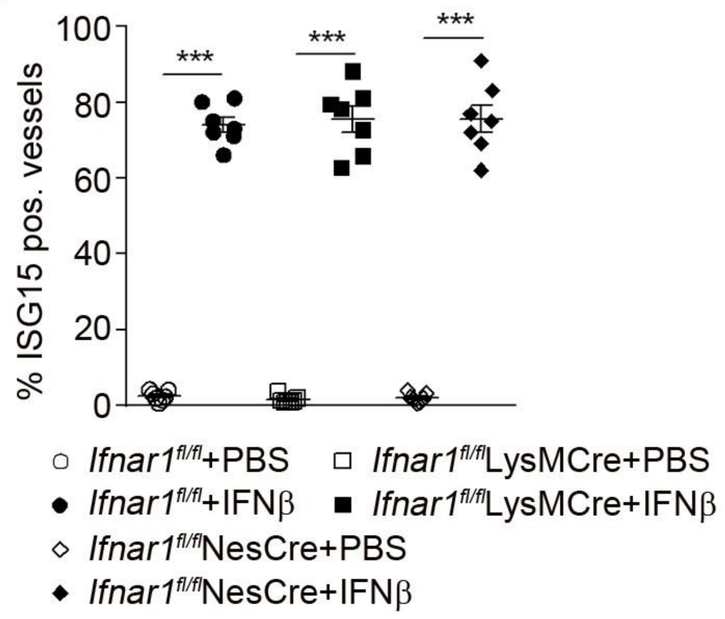

Fig. 4H

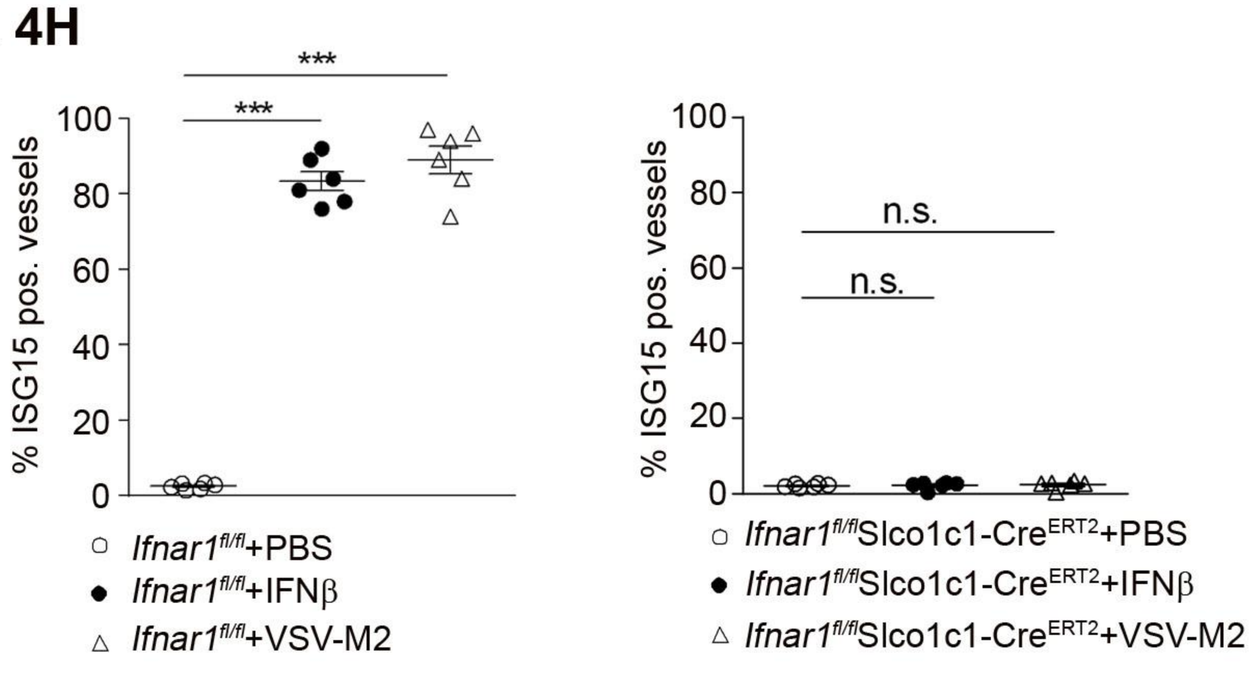

Fig. 5J

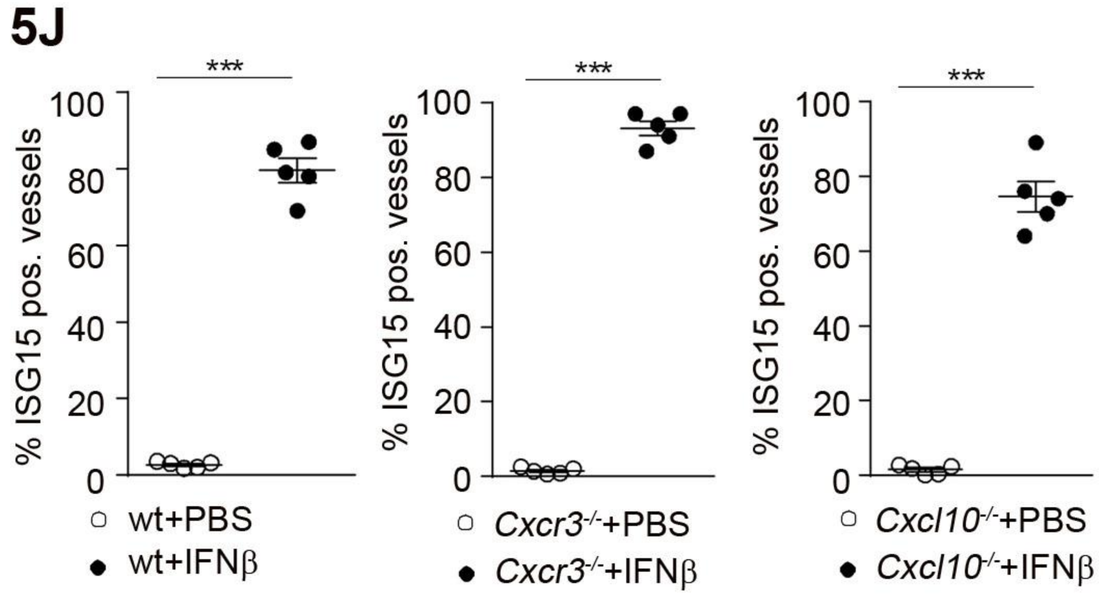

Fig. 5L

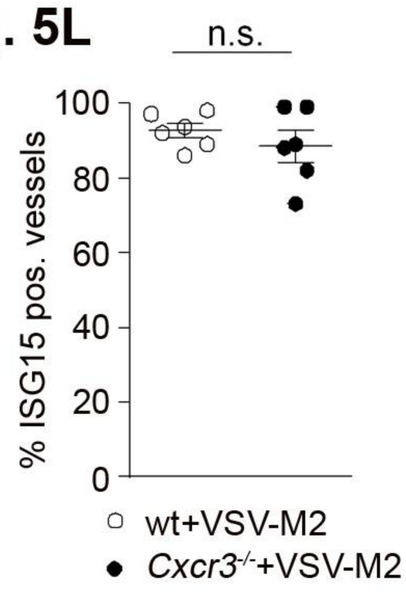

Supplementary Fig. 1

A

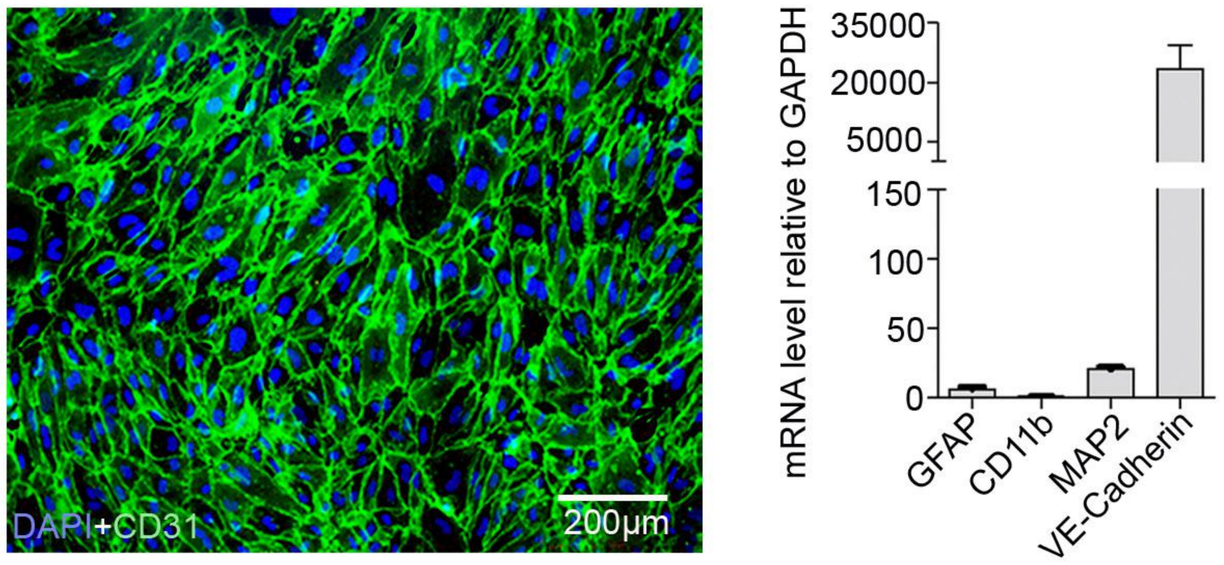

B

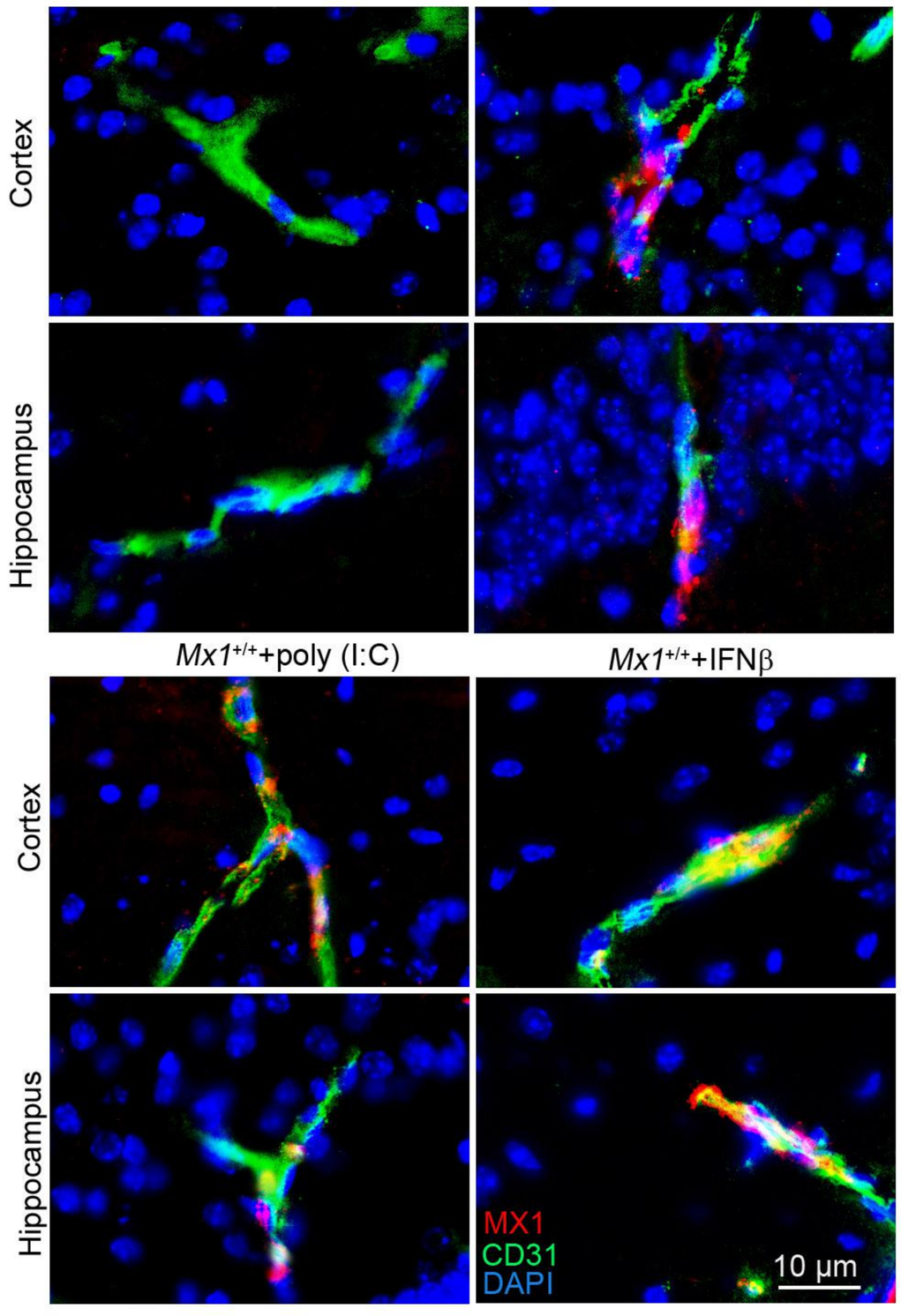

C

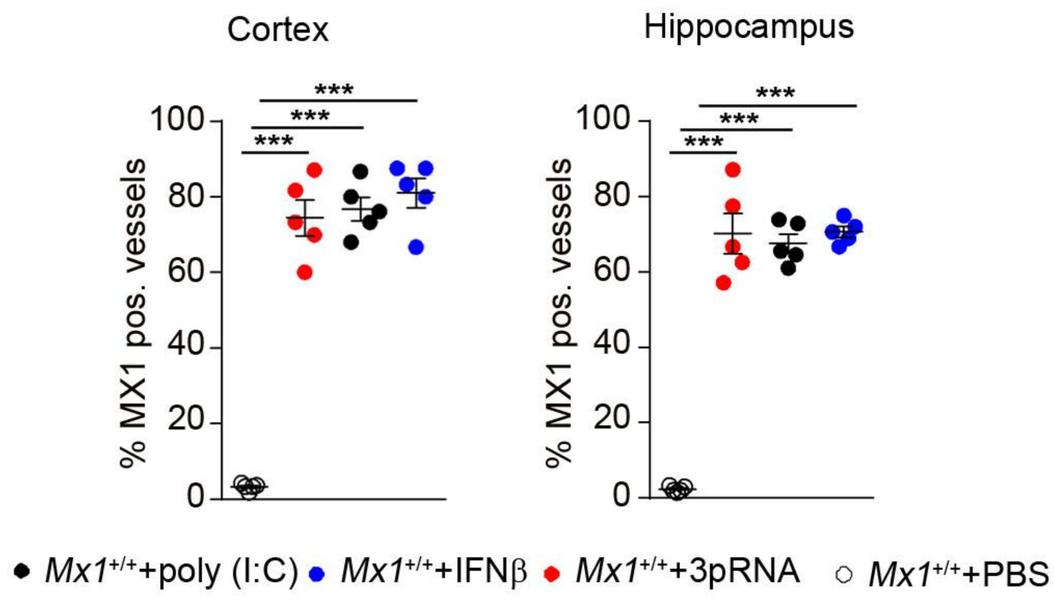

D

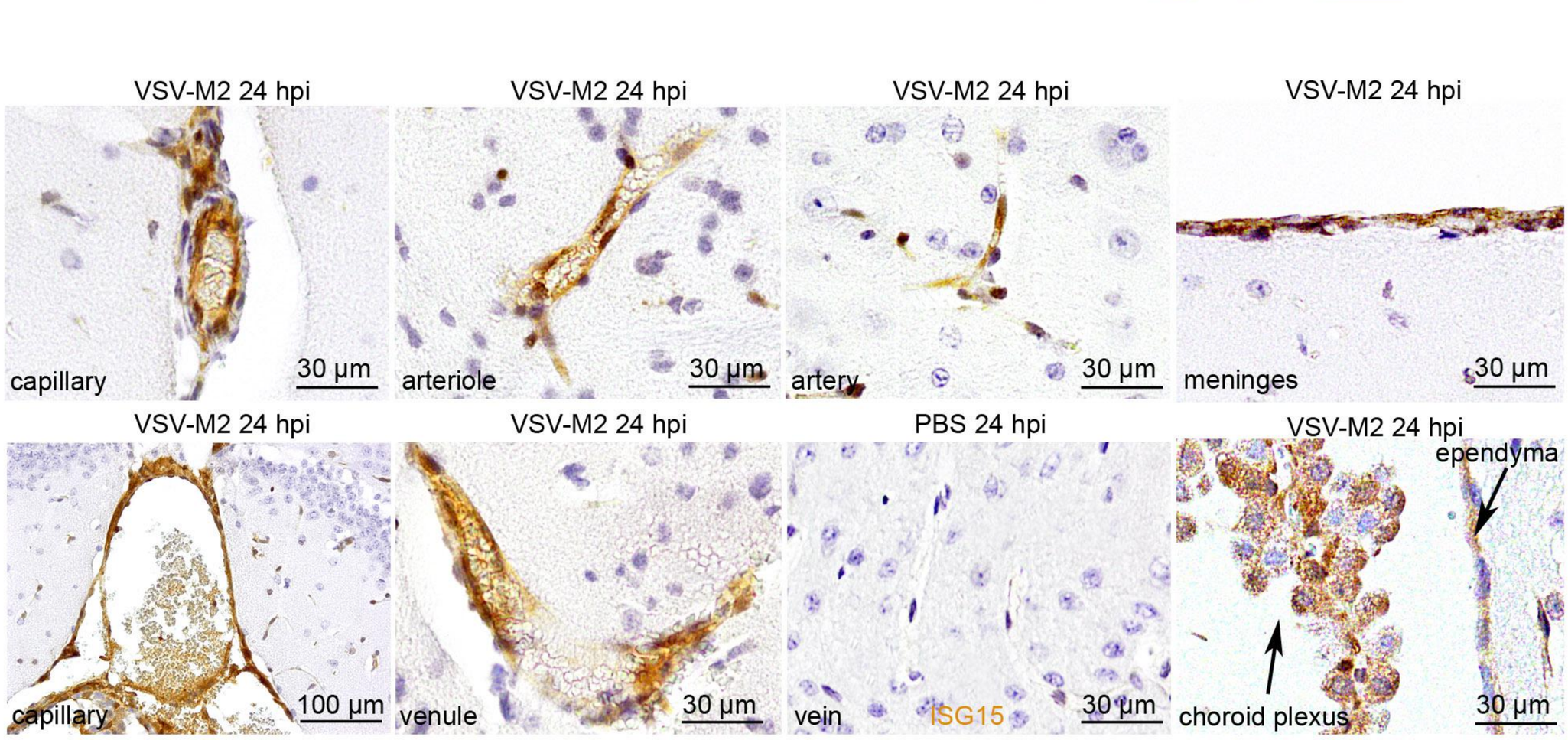

E

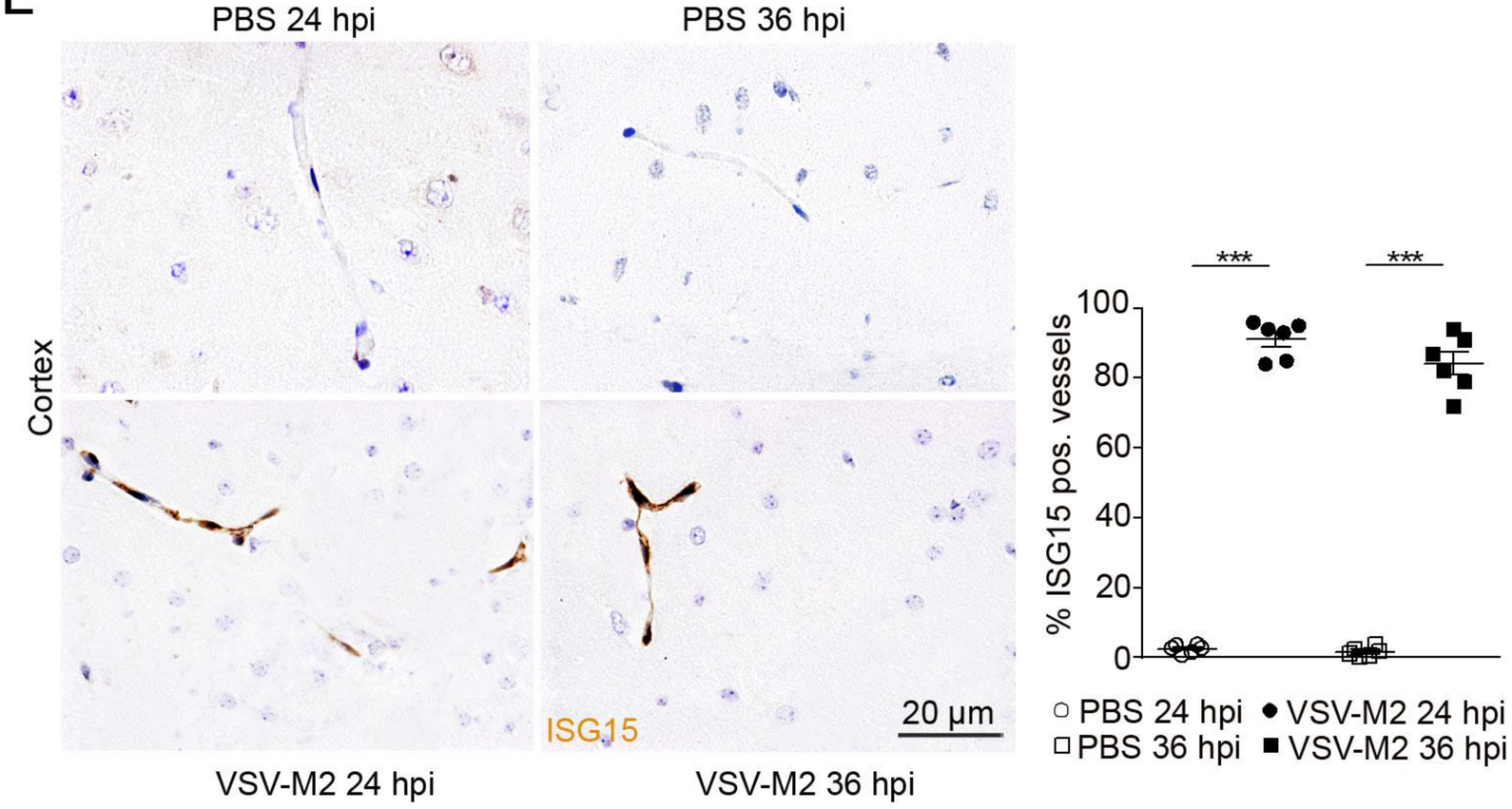

Supplementary Fig. 2

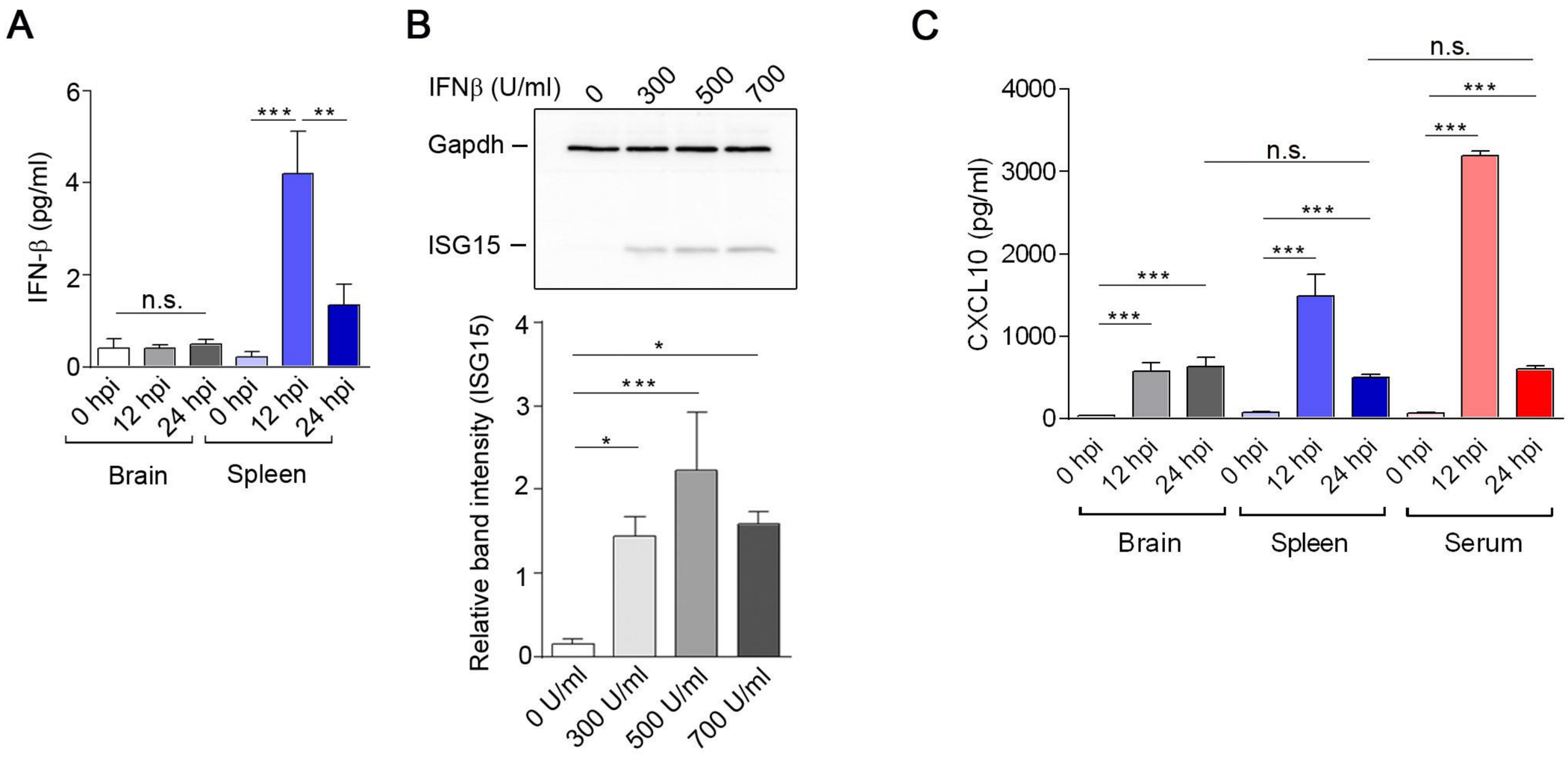

Supplementary Fig. 3

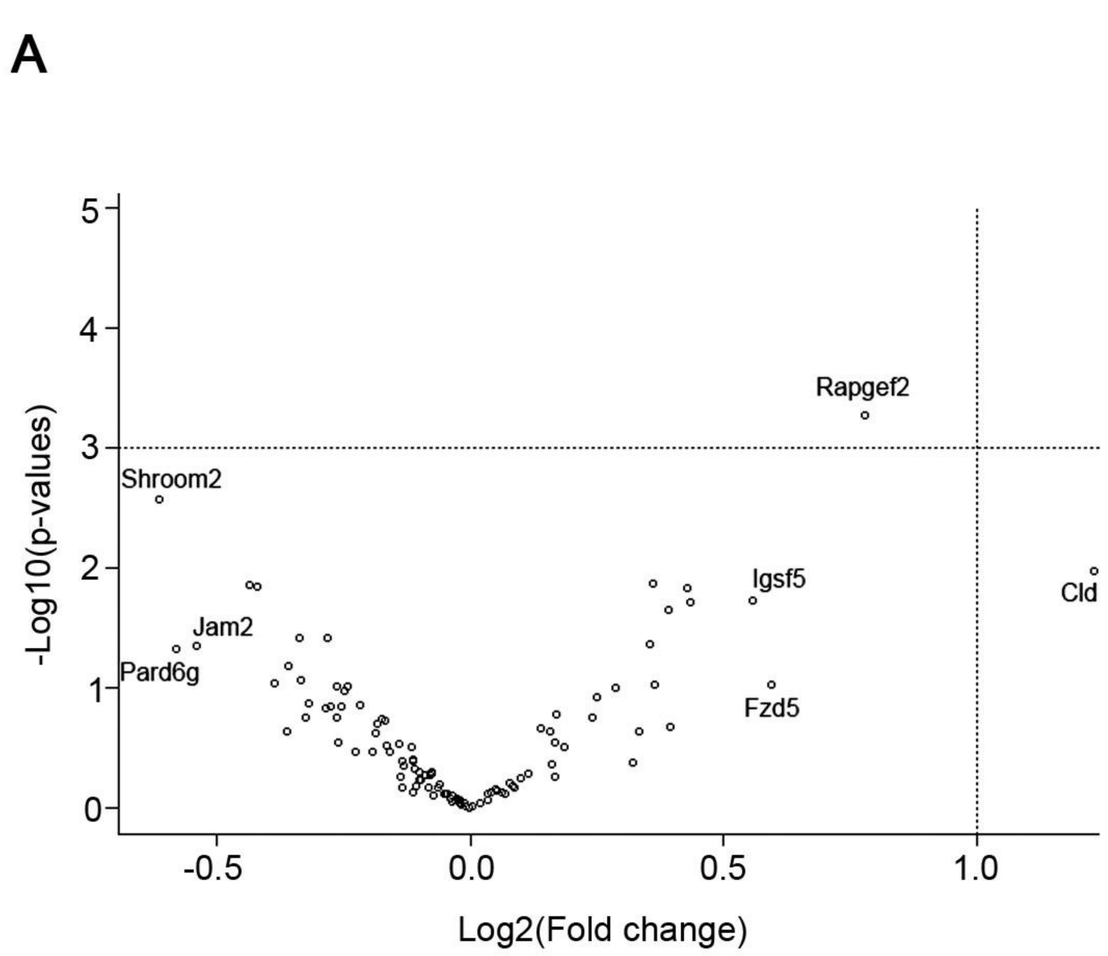

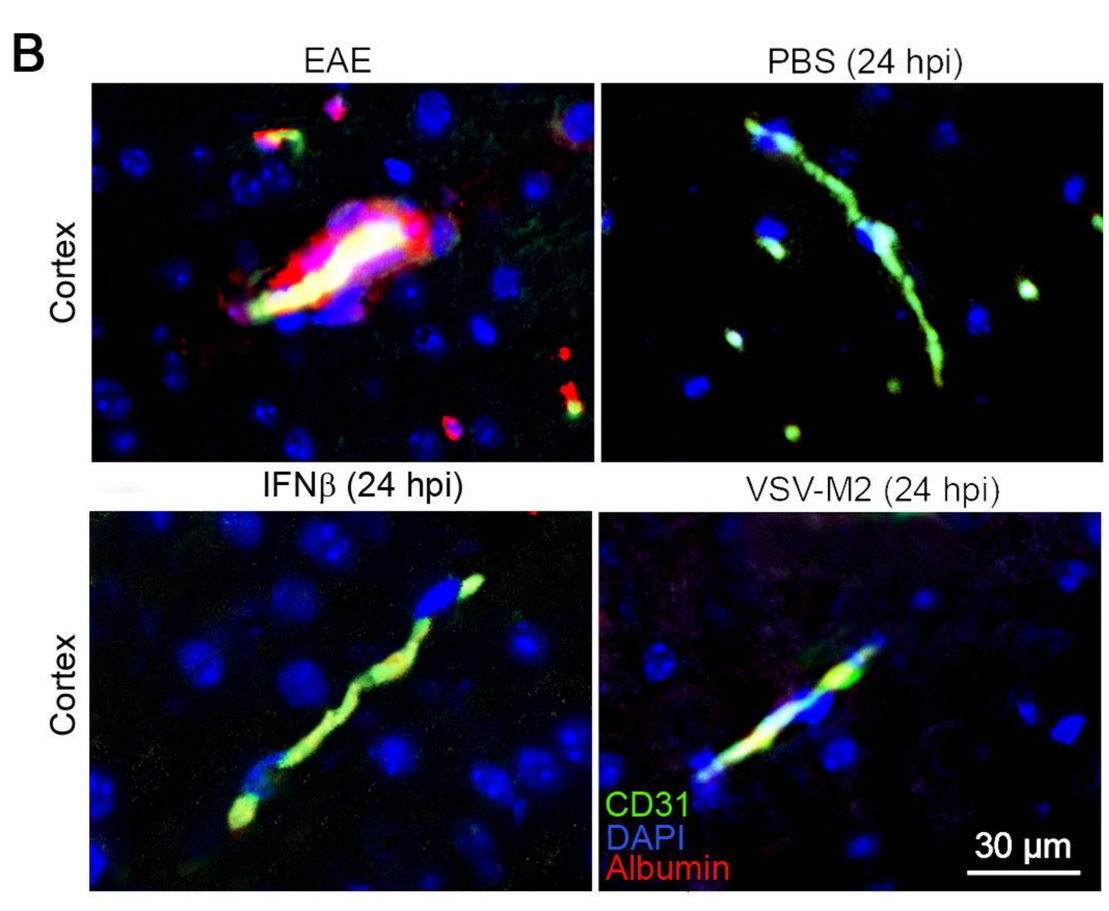

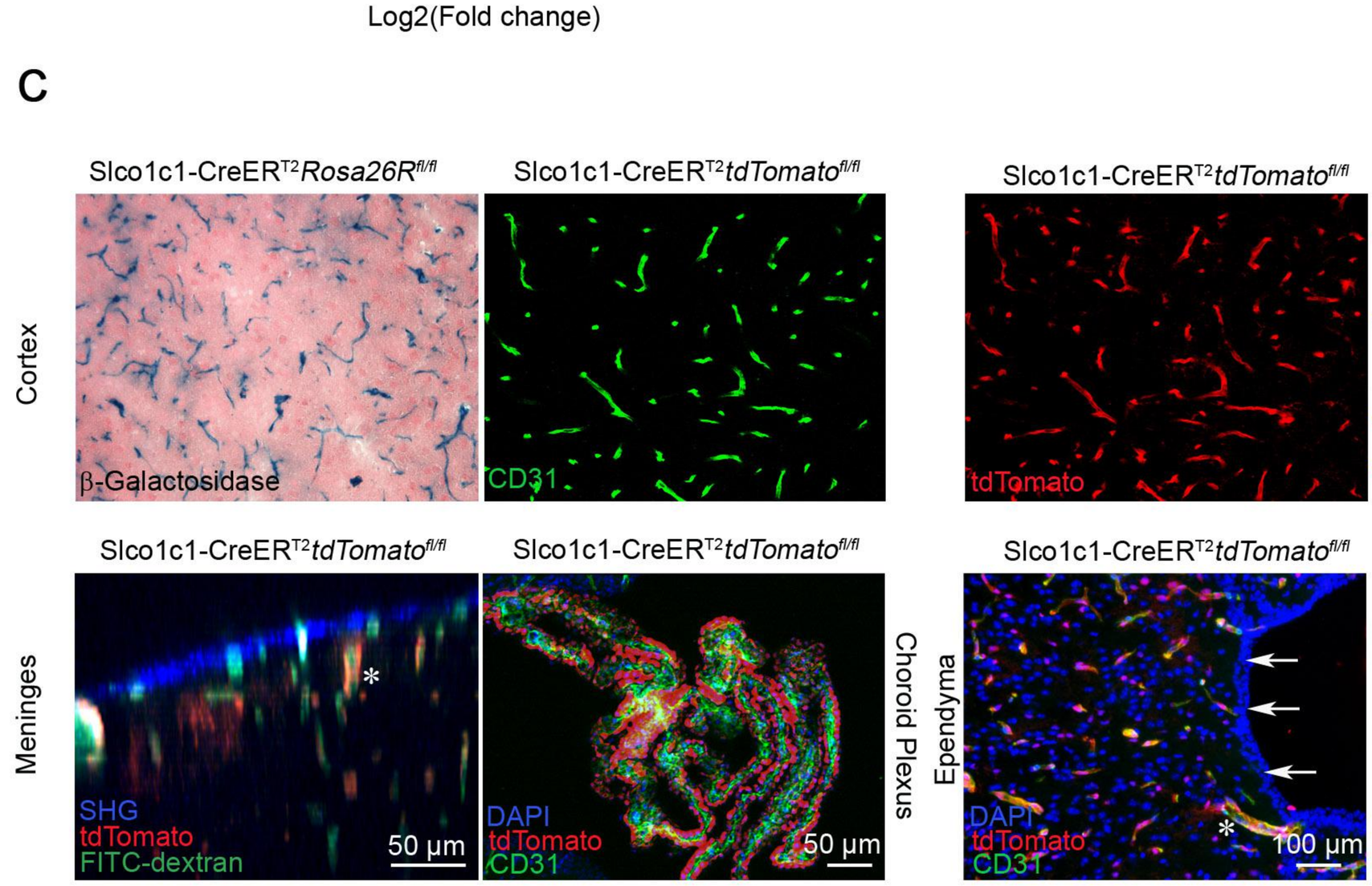

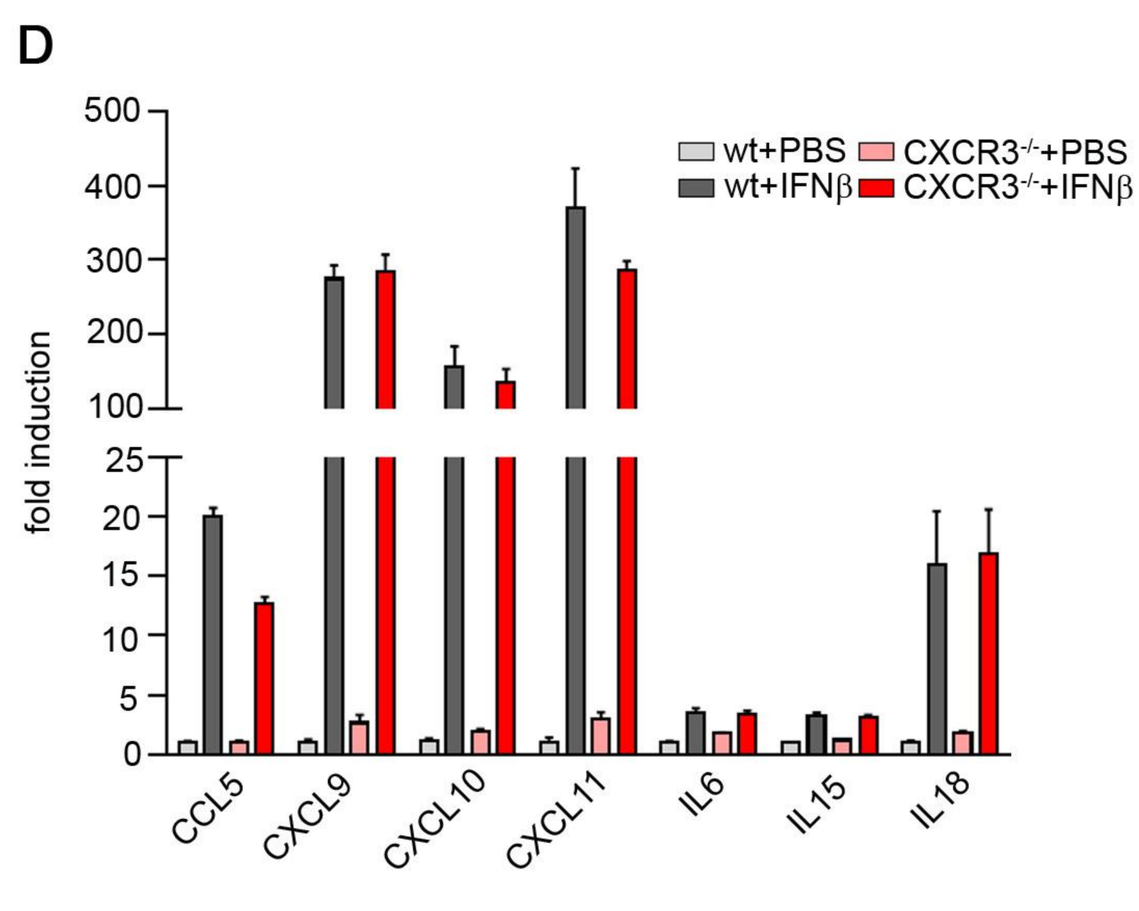

Supplementary Fig. 4

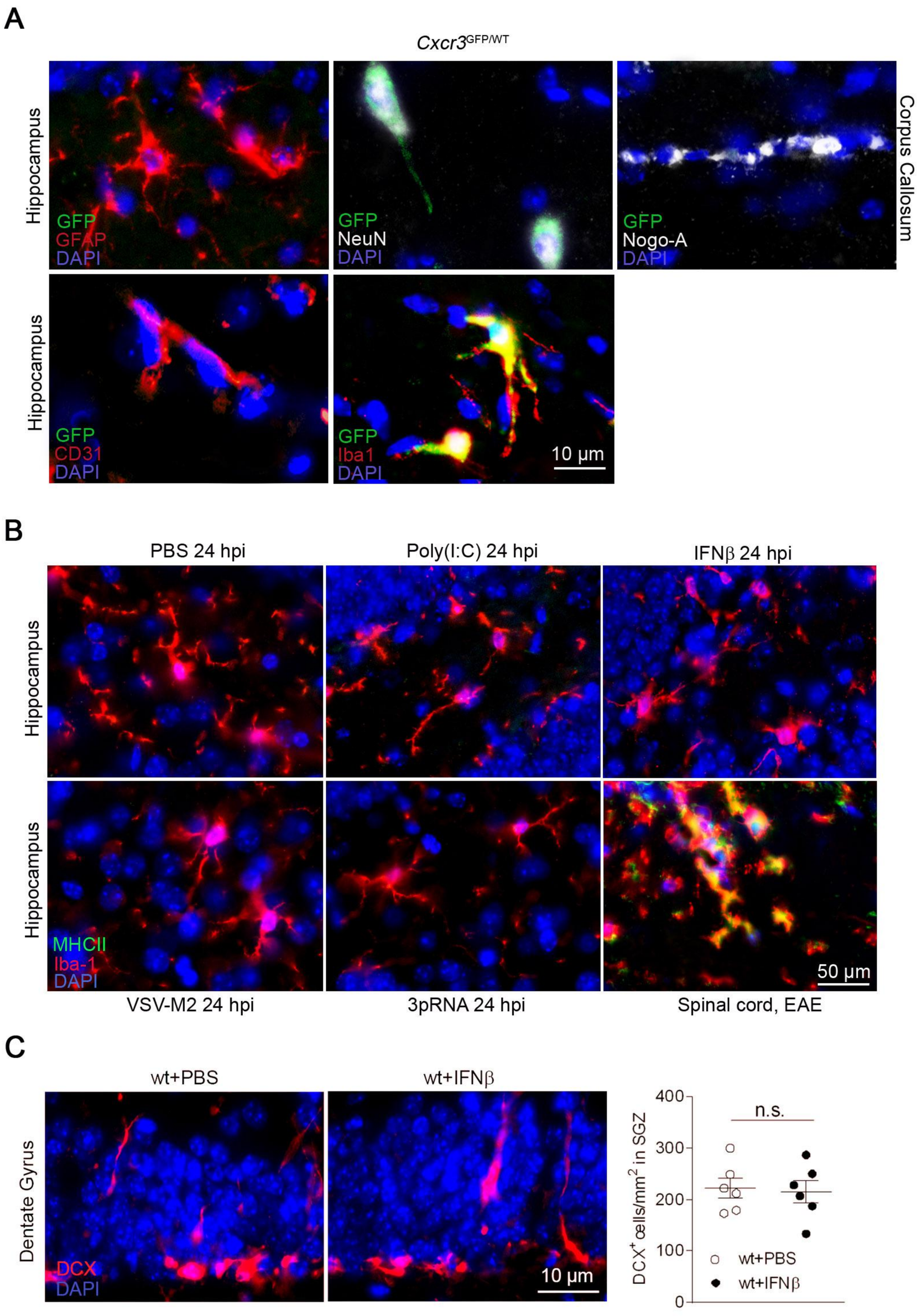

Supplementary Fig. 5

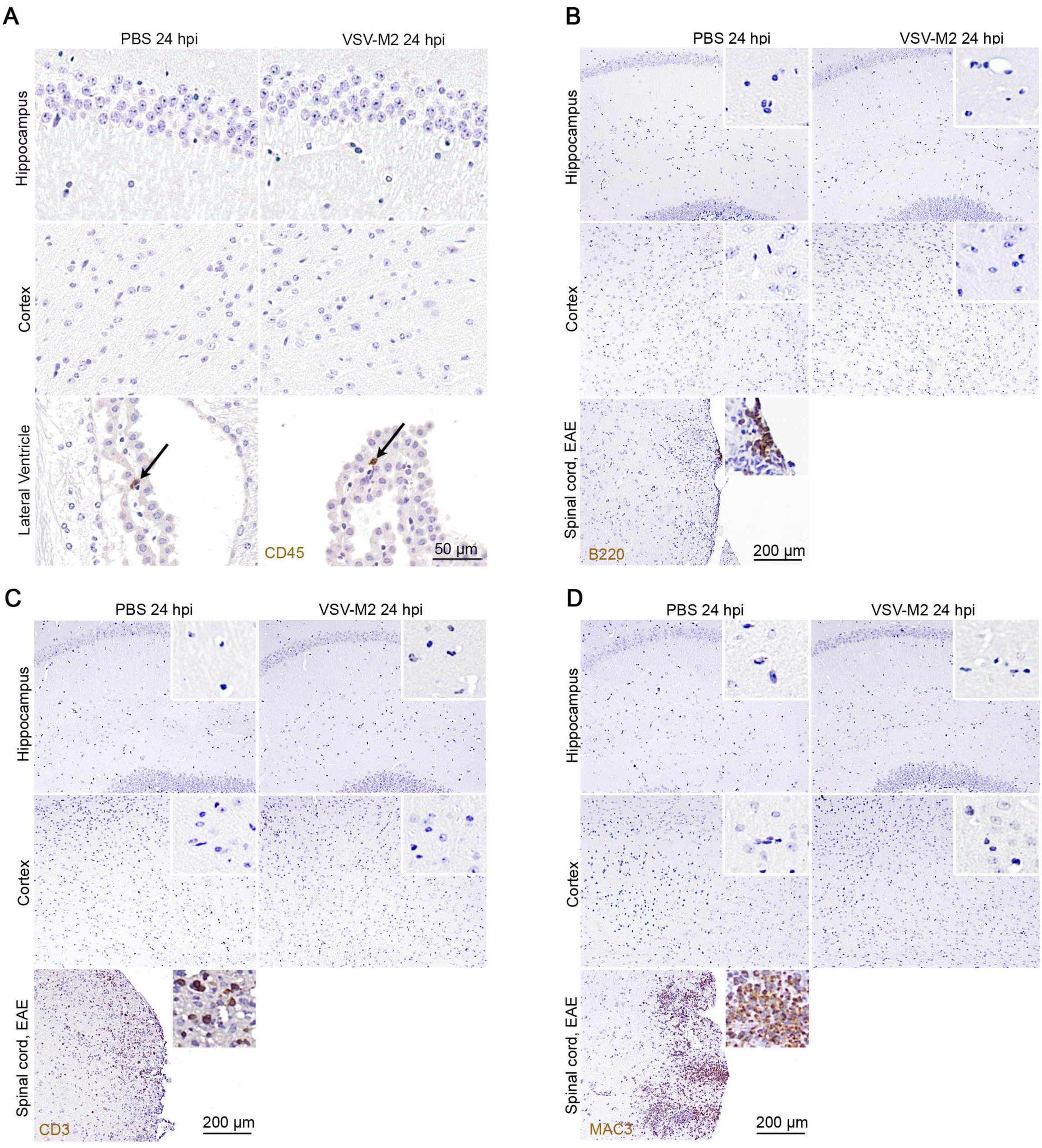

Supplementary Fig. 6

SUPPLEMENTAL DATA

Suppl. Fig. 1: Quantification of ISG15 signals in brain vessels, related to Figures 1-6

The labelling of the graphs corresponds to the label of the respective images in the text. For example, Suppl. Fig.1-2L corresponds to Fig. 2L. Number of symbols in the graph represents number of mice. Two-tailed unpaired *t* test, ***$P < 0.001$; n.s. = non significant.

Suppl. Fig. 2: MX1 or ISG-15 expression in brain endothelial and epithelial cells following activation of type 1 interferon signaling, related to Figures 1,2.

A) Left panel: Cells were isolated from brains of adult wild type mice and stained after 11 days in culture for endothelial marker CD31 (green) and DAPI (blue). Two independent experiments were carried out and one representative image is shown. Right panel: mRNA expression levels of cultured endothelial cells for astrocytic genes (GFAP), microglia (CD11b), neuronal (MAP2) and endothelial (VE-Cadherin) transcripts. Data are expressed as the ration of respective mRNA normalized to endogenous Gapdh and show means ± s.e.m. One representative experiment of three is shown.

B) B6.A2G-Mx1 mice carrying functional *Mx1* alleles were injected with PBS, 3pRNA, poly (I:C) or IFNβ. Brains were removed after 24 h for subsequent immunohistochemical analysis. Nuclear Mx1 staining is seen in red, hippocampal endothelial cells were stained with antibodies against CD34 (green). Nuclei were stained with DAPI (blue). Five mice per group were examined. One representative section is shown.

C) Quantification of MX1-positive vessels in cortex and hippocampus as depicted in Suppl. Fig. 2B. The number of symbols represents number of mice. Colour code indicates different treatments. Two-tailed unpaired *t* test, ***$P < 0.001$.

D) Chromogenic immunohistochemistry of ISG15 in brain endothelia and epithelia of wild-type mice 24 hpi with VSV-M2. Depicted cells were capillaries, arterioles, arteries, and venules as well as meninges, ependyma and epithelial cells of the choroid plexus. One representative picture out of at least three is shown.

E) Immunohistochemical visualization of ISG15 in brain endothelial cells 24 and 36 hpi after PBS or VSV-M2 exposure (left side). Quantification of ISG15-positive vessels expressed as percentage of the total number of vessels. Number of symbols represents number of mice (right side). Two-tailed unpaired *t* test, ***$P < 0.001$.

Suppl. Fig.3: Increased CXCL10 and IFNβ levels after VSV-M2 infection, related to Figures 1, 2, 6.

A) ELISA-based measurement of IFNβ from spleen and brain tissue 0, 12, and 24 hpi with VSV-M2. Data from three independent experiments are shown. Two-tailed unpaired *t* test, ***$P < 0.001$; **$P < 0.01$; n.s. = non significant.

B) ISG15 immunoblot of primary brain endothelial cells (PBECs) cells incubated with recombinant mouse IFNβ for 24 h with the indicated concentrations. Glyceraldehyde 3-phosphate dehydrogenase (GAPDH) was used as loading control. Three independent experiments were carried out with one shown (upper panel). Lower panel: ISG15 quantification. Bars represent the mean ± s.e.m. of the intensity measurement of all experiments compared to the 0 U/mL IFNβ concentration and normalized to the endogenous GAPDH level. (Two-tailed Mann-Whitney *U* test, *$P < 0.05$, ***$P < 0.001$).

C) ELISA-based measurement of CXCL10 in serum, brain tissue and spleen tissue 0, 12 and 24 hpi with VSV-M2. Data from three independent experiments are shown. Two-tailed unpaired *t* test, ***$P < 0.001$; n.s. = non-significant.

Suppl. Fig. 4: Intact and fully functional BBB during different experimental interventions, related to Figures 5, 6.

A) Differential gene analysis was performed on all genes in primary brain endothelia under non-stimulated conditions (PBS) or after IFNβ treatment for 24 h annotated as bicellular tight junction genes in the mouse genome Informatics database. The panel shows a volcano plot showing fold change and *P*-value for each tight junction gene. No significantly upregulated genes (cutoffs 2-fold and $P > 0.001$) were found.

B) Brains of wild-type mice challenged with PBS, IFNβ, or VSV-M2 were stained with the endothelial marker CD31 (green), an antibody against albumin (red) and DAPI (blue) 24 hpi. As a control, brains were stained from mice with experimental autoimmune encephalomyelitis (EAE) at peak of disease. Three independent experiments were carried out and one representative set of images is shown.

C) Histochemical β-galactosidase staining of cortex from *Slco1c1-CreER^{T2}Rosa26RLacZ$^{fl/fl}$* mice treated with tamoxifen. Representative staining from three independent experiments is shown (upper row, far left image). *Slco1c1-CreER^{T2}tdTomato$^{fl/fl}$* mice treated with tamoxifen were subjected to immunostaining with anti-CD31. tdTomato reporter is shown in red. Representative cortical stainings from three independent experiments are shown (upper row). Meninges of tamoxifen-treated *Slco1c1-CreER^{T2}tdTomato$^{fl/fl}$* mice were analyzed with two-photon-microscopy (lower row, far left image). tdTomato reporter is shown in red, FITC-signaling is

depicted in green and SHG-produced signals from collagen in blue. Using the same reporter mice, tdTomato reporter is shown in red, choroid plexus (lower row, middle image) and ependyma (lower row, far right image, arrows) were stained with antibodies against DAPI (blue) and CD31 (green). Asterisks indicate double-positive brain endothelial cells (tdTomato+FITC or tdTomato+CD31, respectively).

D) Quantitative RT-PCR of IFNβ-induced factors in brain endothelial cells after 24 h of treatment. Data are expressed as the ratio of induced factors normalized to endogenous Gapdh compared to unchallenged controls and show means ± s.e.m. One representative experiment of three is shown.

Suppl. Fig. 5: Type 1 interferon signaling has no effect on microglial activation or DCX-positive cell numbers, related to Figures 3, 6.

A) Immunohistochemical staining of hippocampus and corpus callosum (far right image) from *Cxcr3*$^{GFP/WT}$ mice. Brain sections were stained for astrocytes (GFAP), neurons (NeuN), oligodendrocytes (Nogo-A), endothelia (CD31) and microglia (Iba1). CXCR3-GFP is shown in green. One representative staining from six independent experiments is shown.

B) Hippocampal brain sections from wild-type mice injected with PBS, IFNβ, poly(I:C), 3pRNA, or VSV-M2, were stained with antibodies against MHC (major histocompatibility complex) class II (green), an antibody against microglia (red), and DAPI (blue) 24 hpi. As a control, spinal cords were stained from mice with experimental autoimmune encephalomyelitis at peak of disease. Three independent experiments were carried out and one representative image is shown.

C) Immunohistochemical staining of the dentate gyrus from PBS- or IFNβ-injected wild-type mice following MWM testing. Brain sections were stained for doublecortin (DCX, red) and DAPI (blue). One representative staining from six mice per group is shown. Analysis of DCX-positive cells per mm^2 in the subgranular zone (image to the right). Number of symbols represents number of mice. Two-tailed unpaired *t* test, n.s. = non significant.

Suppl. 6: Immunohistochemical visualization of CD45 (A), B220 (B), CD3 (C) and MAC3 (D) in hippocampus and cortex of wild type animals 24 hpi with PBS or VSV-M2, related to Figure 6.

Positive signals for CD45 were visible in the lateral ventricle, for B220, CD3 and MAC3 in the EAE spinal cord positive control at peak of disease. Two independent experiments were carried out with three mice per group. One representative image is shown.

Supplemental Experimental Procedures

Mice: *Ifnar1*$^{-/-}$ mice (Chen et al., 2002) were backcrossed to C57BL/6 at least 20 times. Mice carrying *loxP*-flanked *Ifnar1* (Prinz et al., 2008) were crossed with transgenic mice expressing Cre recombinase under the control of either the LysM (Clausen et al., 1999) or nestin (Tronche et al., 1999) promoter, each back crossed at least 10 times to C57BL/6. Slco1c1-Cre^{ERT2} mice (Ridder et al., 2011) were mated with *Ifnar1*$^{fl/fl}$ mice and were treated with 8 mg tamoxifen (TAM, Sigma) dissolved in 400 µl corn oil (Sigma) injected subcutaneously at two time points 48 h apart. Littermates carrying the respective *loxP*-flanked alleles but lacking expression of Cre- recombinase were similarly injected with 8 mg tamoxifen and used as controls. In some cases Slco1c1-Cre^{ERT2} mice were crossed with the Cre reporter line B6.Cg-Gt(ROSA)26Sor$^{tm14(CAG-tdTomato)Hze}$/J and injected with tamoxifen (Madisen et al., 2010). *Mavs*$^{-/-}$, *Cxcr3*$^{-/-}$, *Cxcl10*$^{-/-}$, and global (Luc-Cre*IFNβ*$^{fl/fl}$) reporter mice were described previously (Dufour et al., 2002; Hancock et al., 2000; Kumar et al., 2006; Lienenklaus et al., 2009). B6.A2G-Mx1 wild type mice carrying intact Mx1 alleles were kindly provided by Peter Staeheli, University of Freiburg (Haller et al., 1995). *Cxcr3*^{GFP} mice (strain name: B6.129S4-*Cxcr3*^{tm1Arsa}/SoghJ) were obtained from The Jackson Laboratory.

Mouse treatments: For VSV-M2 infection (Stojdl et al., 2003), mice were injected intravenously with 2 x 10^6 pfu VSV-M2 or mock infected with PBS and subjected to FST at the indicated time points. For the selective depletion of plasmacytoid dendritic cells (pDCs), mice were treated 24 h before infection with 500 ng αPDCA-1 (Miltenyi Biotec) and at the day of infection (2 x 10^6 pfu VSV-M2) with 200 ng αPDCA-1. One day after infection, FST was carried out. In some experiments, mice were injected with 200 µL of IFNβ solution (10,000 U; endotoxin level of 0.69 EU/mL) in PBS, PBS alone, or PBS containing nucleic acids complexed with jetPEI as described previously (Dann et al., 2012). In summary, 7 µL of *in vivo* jetPEI was mixed with 50 µg of nucleic acids (MWG-BIOTECH AG) at a N:P ratio of 7:1 in a volume of 200 µL of 5 % glucose solution (vol/vol), and incubated for 15 min. Subsequently, 50 µg of complexed 5'-triphosphate RNA, the synthetic dsRNA analog poly(I:C) (Invivogen) was injected. Injections were either done intravenously (poly(I:C), 3pRNA) or intraperitoneally (IFNβ), 4h before each training and test day in the MWM and FST.

Behavioral testing:

The MWM was used to measure spatial learning and memory (Morris, 1984). The apparatus was a black plastic pool with a diameter of 120 cm. A black escape platform (square, 10 × 10 cm) was located 1.0 cm below (hidden) the water surface. The temperature of the water was

kept constant throughout the experiment (20 ± 0.5°C), and a 10 min recovery period was allowed between the training trials. The training consisted of 6 consecutive days of testing, with four trials per day. If the mouse failed to find the escape platform within the maximum time (60 s), the animal was placed on the platform for 10 s by the experimenter. During the first 6 days of testing, the mice were trained with a hidden platform. The platform location was kept constant, and the starting position varied between four constant locations at the pool rim. Mice were placed in the water with their nose pointing toward the wall at one of the starting points in a random manner. On the 7th day, the platform was removed, and the mice were allowed to swim for 60 s to determine their search bias. On testing day 8, mice were trained to find a visible platform, which had a 10 cm high pole with a white flag and was changed every trial to a new position. Timing of the latency to find the visible platform was started and ended by the experimenter. A computer running the *BIOBSERVE* software (BIOBSERVE) analyzed all variables of the MWM test. All behavioral experiments were carried out in double-blind fashion and mice were tested in random order.

Depressive-like behavior was assessed in the FST (Porsolt et al., 1977). For the FST, mice were subjected to swim sessions in individual glass cylinders (height, 39 cm; diameter, 21.7 cm) containing water 15-cm deep at 23-25°C. On day 1, all animals were placed in the cylinder for a pre-swim session of 15 min. On the test day 24 h later (day 2), the mice were subjected to a test swim session for 7 min. The water was changed between subjects. The behavioral measure scored by a blinded experimenter was the duration of immobility. A mouse was judged to be immobile when making only those movements necessary to keep its head above water.

Electrophysiology (*in vitro*): For extracellular field recordings, horizontal brain slices of 400 µm thickness were obtained in ice-cold artificial cerebrospinal fluid (aCSF) with a VT1000S vibratome (Leica Biosystems) and allowed to recover at 34^{o}C interface condition (Kann et al., 2011). aCSF consisted of: 129 mM NaCl, 1.25 mM NaH_2PO_4, 10 mM D-Glucose, 1.8 mM $MgSO_4$, 3 mM KCl, 1.6 mM $CaCl_2$, 26 mM $NaHCO_3$. Both, aCSF and the interface atmosphere were aerated constantly with carbogen (95 % oxygen, 5 % carbon dioxide) throughout the preparation, recovery, and experiment. All electrophysiological measurements took place at 34^{o}C interface condition, with 1.5 mL/min flow rate of bubbled aCSF. For patch-clamp recordings, transversal hippocampal slices of 350 µm were cut with a VT1200S vibratome (Leica) and allowed to recover in aCSF (Kirchheim et al., 2013). Field potential recordings were conducted in the presence of vehicle 0.001 % bovine serum albumin or 10 ng/ml CXCL10 (IP-10) (PeproTech) + vehicle starting with a 35 min wash-in period.

Field excitatory postsynaptic potentials (fEPSPs) recorded in the dendritic layer (stratum radiatum) of the hippocampal CA1 subregion were elicited via bipolar electrical stimulation of

the fibers between CA3 and CA1 with platinum-wire microelectrodes (diameter 0.025 mm). The synaptic efficacy was characterized by the amplitude of fEPSPs in response to stimuli of progressively increasing intensity . Triplets of paired-pulses with inter-stimulus intervals varying from 200, 100, 50 to 20 ms were adjusted to elicit 50 % sub-maximum fEPSP response . For determination of synaptic LTP, whole-cell patch-clamp recordings were collected from CA1 pyramidal neurons identified via video microscopy (Axioskop2 FS with AxioCam ICm1, Zeiss, Oberkochen, Germany). Data were sampled at room temperature (23-26 °C) via the amplifier SEC05LX in bridge mode (NPI, Tamm, Germany) and PatchMaster software (Heka, Lambrecht, Germany). During recordings, slices were superfused with aCSF containing: 125 mM NaCl, 25 mM $NaHCO_3$, 2.5 mM KCl, 1.25 mM NaH_2PO_4, 2 mM $CaCl_2$, 1 mM $MgCl_2$, and 25 mM glucose (equilibrated with carbogen). Patch-pipettes (tip resistance 4.3 ± 0.1 MΩ) contained the following solution: 120 mM KGlu, 20 mM KCl, 10 mM HEPES, 4 mM Mg_2ATP, 2 mM Na_2GTP, and 10 mM Na_2P-creatine (pH 7.34). Patch- and double barrel stimulation pipettes were pulled from borosilicate glass (Hilgenberg, Malsfeld, Germany) using a DMZ-universal puller (Zeitz, Martinsried, Germany). For extracellular Schaffer collateral stimulation, pipettes (tip size ~50 µm) filled with aCSF were placed into the stratum radiatum and bipolar voltage pulses (0.1 ms) were applied to evoke excitatory postsynaptic potentials (EPSPs; mean amplitude, 4.5 ± 0.4 mV at -69.4 ± 0.9 mV). A 10 min EPSP baseline was recorded at 0.05 Hz and LTP was induced via a theta burst stimulation (TBS) protocol consisting of 4 sweeps (inter-sweep interval 10 s); each containing 10 presynaptic stimulation bursts at theta frequency (inter-burst interval 200 ms). Each burst consisted of a 100 ms train of 100 Hz presynaptic stimulations, paired with a 55 ms delayed postsynaptic (intracellular) stimulation train of 5 ms depolarizations (1.5 nA) also at 100 Hz. The amount of LTP was quantified as averaged EPSP amplitudes (10-30 min after TBS) relative to respective pre-TBS (10 min) traces. The 12 analyzed CA1 cells had the following properties: input resistance, 191.4 ± 17.9 MΩ; capacitance, 105.2 ± 7.8 pF; resting potential, -67.2 ± 1.0 mV, and these parameters were not different among the compared groups (control, CXCL10, n = 6, respectively).

Electrophysiology (*in vivo*): The present study was carried out in accordance with the European Communities Council Directive of September 22nd, 2010 (2010/63/EU) for care of laboratory animals and after approval of the local ethics committee (Bezirksamt Arnsberg). Male C57/BL6 mice (7-8 weeks, Charles River, Germany) were anaesthetized (sodium pentobarbital 60 mg/kg, i.p.) and underwent stereotaxic chronic implantation of bipolar stimulating electrodes in the right Schaffer collateral pathway of the dorsal hippocampus (anterioposterior (AP): -2.0 mm; mediolateral (ML): 2.0 mm from bregma; dorsoventral (DV): ~1.4 mm from brain surface) and monopolar recording electrodes in the ipsilateral CA1

stratum radiatum (AP: -1.9; ML: 1.4; DV: ~1.2), as described previously (Buschler et al., 2012). A cannula was chronically implanted into the lateral cerebral ventricle (AP: -0.3; ML: 0.9; DV: -2.3). This was made by removing the stainless injection needle from a hypodermic needle (25 gauge, Braun GmbH, Germany), and then smoothing the ends by grinding. The outer diameter of the cannula was 0.5 mm and the length was 2.5 mm. Following insertion of the electrodes and cannula, the entire assembly was stabilized with dental acrylic, as described previously (Buschler et al., 2012). Ten to fourteen days after electrode implantation, field excitatory post synaptic potentials (fEPSPs) were revoked by means of test-pulse stimulation (0.025Hz) of freely behaving mice, as described previously (Buschler et al., 2012). During the experiment, each time-point consisted of the average of 5 consecutively evoked fEPSP responses at 40 s intervals. The first 6 time-points, which were recorded at 5 min intervals, were averaged, and all time points throughout the experiment were expressed as a mean percentage (± standard error of the mean) of this value. After 30 min of baseline recordings (6 time points) IP-10 or vehicle were applied. IP-10 was dissolved in 0.9% NaCl and applied via the implanted cannula in a 80 ng dose in a 2 μL injection volume over a 6 minute period, according to established methods (Manahan-Vaughan, 1997). The experiments were conducted under “blind” conditions.

To induce LTP, afferent stimulation at 100 Hz (50 pulses x 4 trains, 5 min apart) was applied immediately after the twelfth time-point. On the next day, roughly 24 h after the experiment began, a further recording lasting for 1 h was performed to observe the persistency of any plasticity changes induced. The fEPSP was quantified by measuring the slope obtained on the first negative deflection of the evoked potential. By means of an input-output curve, determined before every experiment, the largest obtainable fEPSP was found for each individual animal (maximum intensity used 125 μA). The intensity that elicited 40 % of the maximum fEPSP was used for recordings.

Statistical analysis was conducted using a factorial analysis of variance (ANOVA) followed by post-hoc Fisher LSD test and Student’s *t*-test. The fEPSPs from the period after electrical stimulation with or without the drug treatment to the end of the experiment was compared. The significance level was set at $P < 0.05$.

qRT-PCR: The following primers were used: GFAP: forward 5′-ATCGAGATCGCCACCTACAG-3′, reverse 5′-CTCACATCACCACGTCCTTG-3′; CD11b: forward 5′-CAGATCAACAATGTGACCGTATGGG-3′, reverse 5′-CATCATGTCCTTGTACTGCCGCTTG-3′; forward MAP2: 5′-CCACCTGAGATTAAGGATCA-3′, reverse 5′-GGCTTACTTTGCTTCTCTGA-3′; VE cadherin: forward, 5′-ACGGACAAGATCAGCTCCTC-3′, reverse 5′-TCTCTTCATCGATGTGCATT-3′; GAPDH: forward 5′-CGACTTCAACAGCAACTCCCACTCTTCC-3′, reverse 5′-

TGGGTGGTCCAGGGTTTCTTACTCCTT-3′; IFNAR1: forward 5′-GCCCTGCTGAATAAGACCAG-3′, reverse 5′-GTGGGAAGCACACATGACAC-3′ IL-18: forward 5′-GACTCTTGCGTCAACTTCAAGG-3′, reverse 5′-CAGGCTGTCTTTTGTCAACGA-3′; CXCL-9: forward 5′-TGGAGTTCGAGGAACCCTAGT-3′; reverse 5′-GAGTCCGGATCTAGGCAGGT-3′; CXCL11: forward 5′-CCACAGCTGCTCAAGGCTTCCT-3′, reverse 5′-GCGAGCTTGCTTGGATCTGGGG-3′; CXCL10: forward 5′-TGCTGGGTCTGAGTGGGACT-3′, reverse 5'-CCCTATGGCCCTCATTCTCAC-3′; CCL5: forward 5′-TGCCCACGTCAAGGAGTATTT-3′, reverse 5′-TCTCTGGGTTGGCACACACTT-3′; IL-6: forward 5′-CCGGAGAGGAGACTTCACAG-3′, reverse 5′-GGTAGCATCCATCATTTCTTTG-3′; IL15: forward 5′-GAATACATCCATCTCGTGCTACT-3', reverse 5'-ATAAGGCTTTCAATTTTCTCC-3′; CCL2: forward 5′-TCTGGGCCTGCTGTTCAC-3′, reverse 5′-TTGGGATCATCTTGCTGGTG-3′; OAS2: forward 5′-GACCGTCCTGGACCTGGTTA-3′, reverse 5′-GGGTCTGCATTACTGGCACT-3′; OASL1: forward 5′-CAGGGGACAAAGGCCTATCA-3′, reverse 5′-CACGGTCACCTGGATATCGG-3′; SLFN4: forward 5′-GATGGATGGCGTCGTGGAAAG-3′, reverse 5′-ACCAGTTCAGCGTAGTCCGT-3′; USP18: forward 5′-TCGTCCAGCCCAAAGAGTTAG-3′, reverse 5'-AAAGACCAAGCCTTCCGTGTG-3′.

Histology: In summary, following perfusion, brains were removed and fixed in 4 % buffered formalin. Paraffin-embedded 3 µm sections were deparaffinized, and were incubated in 3 % H_2O_2 in methanol and subsequently in 70 % ethanol. Brain sections were stained overnight with the following primary antibodies: goat anti-DCX (1:200; Santa Cruz Biotechnology), mISG15 (Osiak et al., 2005) (1:500, kindly provided by Klaus-Peter Knobeloch, University of Freiburg, Freiburg, Germany), rat anti-CD34 antibodies (1:50, clone MEC14.7; BioLegend) (Zaynagetdinov et al., 2011), rat anti-CD31 (1:400, BD Pharmingen), and anti-mCXCL10 (1:200, R&D Systems) (Campanella et al., 2008). Secondary antibodies were added as follows: Alexa Fluor 488, 1:500; Alexa Fluor 568, 1:500, for 2 h at room temperature. Nuclei were counterstained with DAPI. Images were taken using a conventional fluorescence microscope (Olympus BX-61).

Endothelial cell cultures: Mice were sacrificed with a lethal dose of anesthetic, and the cerebrum was isolated and dissected free of the meninges. The brain was homogenized in a Dounce homogenizer, and the resulting homogenate was centrifuged at 4,000 g for 5 min. The pellet was resuspended in 18% dextran solution (molecular weight: 64,000-76,000, Sigma-Aldrich) in DMEM (Gibco) and centrifuged at 6,000 g for 10 min. After removing the supernatant and myelin debris, the pellet was resuspended in DMEM containing 1 mg/mL collagenase/dispase (Roche), 40 µg/mL DNase 1 (Roche), and 0.147 µg/mL tosyllysine

chloromethyl ketone (Sigma-Aldrich), and incubated at 37°C for 75 min with occasional agitation to free endothelial cells from pericytes, perivascular macrophages, and remains of the basement membrane. The cell suspension was centrifuged at 4,000 g for 5 min, the supernatant was discarded, and cells were washed and seeded in 6-well plates coated with mouse collagen IV (BD). Cells were subsequently grown in DMEM-F12 (Gibco) supplemented with 10 % fetal bovine serum (PAA Laboratories), 2 mM L-glutamine, 100 IU/mL penicillin, 100 µg/mL streptomycin, 15 U/mL heparin (Biochrom), and 30 µg/mL of endothelial cell growth supplement (Sigma-Aldrich). 4 µg/mL puromycin (Sigma-Aldrich) was added for the first 48 h after preparation to deplete cells of non-endothelial origin. Additionally, primary endothelial cells from heart and lung tissue were isolated. The organs were removed, digested with 2 mg/mL collagenase/dispase, and passed through a 70 µm cell strainer. Fc receptors were blocked with 1 µg/mL CD16/32 antibodies (eBioscience). Biotinylated antibodies against CD105 and CD31 (1 µg/mL, eBioscience) were added and labelled with α-biotin microbeads (Miltenyi Biotec) for MACS separation. The cells were cultured as described for the PBECs. To prepare primary mixed cortical cultures, cortices of adult mice were dissected, homogenized, and digested with trypsin and DNase I. Cells were grown in DMEM-F12 supplemented with 10 % FCS, 100 IU/ml penicillin, 100 µg/mL streptomycin, and 0.5 mM L-glutamine. For immunohistochemical detection of PBECs, cell cultures were stained with antibodies against CD31 1:300 (BD) (Ridder et al., 2011). Nuclei were counterstained with DAPI. Fluorescent images were taken using a conventional fluorescence microscope (Olympus BX-61). Purity of endothelial cell culture was determined by qRT-PCR.

Two-photon microscopy: The mouse was anesthetized with urethane (1.8 mg/g body weight) and kept at 37°C body temperature. After injecting Fluorescein isothiocyanate (FITC) dextran (150 kD, 0.2 mg/g body weight in 100 µL, TdB consultancy) to visualize the vasculature, an open cranial window was drilled and covered with an artificial tears gel (Bausch & Lomb) to bridge the working distance of the water immersion objective used. Images were acquired with a two-photon microscope (DermaInspect, JenLab) equipped with a tunable infrared femtosecond-laser (Wide Band MaiTai; Spectra Physics). An image stack of 0.3 x 0.3 x 0.2-mm volume was scanned during excitation with a wavelength of 900 nm. Emitted light was split, resulting in green fluorescence (FITC dextran, 500-550 nm) and red fluorescence (recombined cells expressing tdTomato, >570nm). In addition, a second harmonic generated (SHG) signal was recorded at 450 nm, which reflects the collagen structure of the meninges at the surface of the brain.

Luciferase measurements: For *ex vivo* luciferase measurements, tissue was homogenized in 10 µL/g GLO lysis buffer (Promega) using FastPrep-24 equipment and lysing matrix A (MP Biomedicals). Samples were centrifuged, 20 µL of cleared supernatant was mixed with an equal volume of luciferin (Bright-Glo™ Luciferase Assay System, Promega), and luciferase activity was measured in a plate luminometer (Berthold Technologies).

Microarray: Affymetrix GeneChip array data was pre-processed using Affymetrix Expression Console and normalized through the Robust Multi-array Average (RMA) implementation in the Expression Console. Differential ontology analysis was carried out using BRB-ArrayTools developed by Dr. Richard Simon and the BRB-ArrayTools Development Team. Gene Ontology Analysis was performed using GOrilla (Eden et al., 2007; Eden et al., 2009) and REViGO (Supek et al., 2011) tools. Visualization was performed using Cytoscape (Shannon et al., 2003). Venn diagrams were created by intersection of gene lists exported from BRB Tools into a Webtool provided by the Bioinformatics & Evolutionary Genomics group of Prof. van de Peer at the University of Ghent.

Quantification of DCX-positive cells: Cells were counted using the optical fractionator, a method for unbiased stereological analysis. This method was performed using a computer-assisted image analysis system, consisting of an Axiophot photomicroscope (Zeiss) equipped with a computer-controlled motorized stage, a video camera, and the Stereo Investigator software (MicroBrightField, Williston, VT). The number of positive cells throughout the rostrocaudal extent of the dentate gyrus was counted with a coded one-in-nine series for frozen sections of 30 µm thickness. We used a modified version of the optical fractionator method as reported previously (West et al., 1991) and as used and cited in a recent report (Gould et al., 1999). The total numbers of positive cells were multiplied by 9 and reported as total number of cells per dentate gyrus.

Statistical analysis: To obtain unbiased data, experimental mice of all relevant genotypes were processed together and cell quantifications were carried out blinded to the genotype. Only after finalization of all quantitative measurements were the samples allocated to their genotypes. In all behavioral assays, subjects were randomly assigned to a group and the experiments were blind with respect to group assignments. No statistical methods were used to predetermine sample sizes and exact group numbers were determined by animal availability. However, we did ensure that our sample sizes were similar to those generally employed in the field and all experiments were replicated at least once. No data or mice (n) were excluded. Statistical analysis was performed using GraphPad Prism (GraphPad Software, Version 6.0). For comparisons between multiple groups, ANOVA was used followed by individual *post hoc* tests when applicable. In some cases significance was

indicated by multiple rows of asterisks directly above the MWM graphs. Each row of asterisks starting from the top represents the relevant significance level when compared to the respective control at the indicated day as seen from the top. Electrophysiological data were analyzed using Wilcoxon signed ranksum test and F-test. For statistical analysis of all other experiments, all data were tested for normality applying the Kolmogorov-Smirnov test. If normality was given, an unpaired two-tailed *t*-test was applied. If the data did not meet the criteria of normality, the Mann-Whitney *U* test was applied. Values are expressed as mean ± SEM with significance determined at $P < 0.05$.

SUPPLEMENTAL REFERENCES

Buschler, A., Goh, J.J., and Manahan-Vaughan, D. (2012). Frequency dependency of NMDA receptor-dependent synaptic plasticity in the hippocampal CA1 region of freely behaving mice. Hippocampus *22*, 2238-2248.

Campanella, G.S., Tager, A.M., El Khoury, J.K., Thomas, S.Y., Abrazinski, T.A., Manice, L.A., Colvin, R.A., and Luster, A.D. (2008). Chemokine receptor CXCR3 and its ligands CXCL9 and CXCL10 are required for the development of murine cerebral malaria. Proc Natl Acad Sci U S A *105*, 4814-4819.

Chen, L.F., Mu, Y., and Greene, W.C. (2002). Acetylation of RelA at discrete sites regulates distinct nuclear functions of NF-kappaB. The EMBO journal *21*, 6539-6548.

Clausen, B.E., Burkhardt, C., Reith, W., Renkawitz, R., and Forster, I. (1999). Conditional gene targeting in macrophages and granulocytes using LysMcre mice. Transgenic Res *8*, 265-277.

Dann, A., Poeck, H., Croxford, A.L., Gaupp, S., Kierdorf, K., Knust, M., Pfeifer, D., Maihoefer, C., Endres, S., Kalinke, U., *et al.* (2012). Cytosolic RIG-I-like helicases act as negative regulators of sterile inflammation in the CNS. Nat Neurosci *15*, 98-106.

Dufour, J.H., Dziejman, M., Liu, M.T., Leung, J.H., Lane, T.E., and Luster, A.D. (2002). IFN-gamma-inducible protein 10 (IP-10; CXCL10)-deficient mice reveal a role for IP-10 in effector T cell generation and trafficking. J Immunol *168*, 3195-3204.

Eden, E., Lipson, D., Yogev, S., and Yakhini, Z. (2007). Discovering motifs in ranked lists of DNA sequences. PLoS computational biology *3*, e39.

Eden, E., Navon, R., Steinfeld, I., Lipson, D., and Yakhini, Z. (2009). GOrilla: a tool for discovery and visualization of enriched GO terms in ranked gene lists. BMC bioinformatics *10*, 48.

Gould, E., Beylin, A., Tanapat, P., Reeves, A., and Shors, T.J. (1999). Learning enhances adult neurogenesis in the hippocampal formation. Nat Neurosci *2*, 260-265.

Haller, O., Frese, M., Rost, D., Nuttall, P.A., and Kochs, G. (1995). Tick-borne thogoto virus infection in mice is inhibited by the orthomyxovirus resistance gene product Mx1. J Virol *69*, 2596-2601.

Hancock, W.W., Lu, B., Gao, W., Csizmadia, V., Faia, K., King, J.A., Smiley, S.T., Ling, M., Gerard, N.P., and Gerard, C. (2000). Requirement of the chemokine receptor CXCR3 for acute allograft rejection. J Exp Med *192*, 1515-1520.

Kann, O., Huchzermeyer, C., Kovacs, R., Wirtz, S., and Schuelke, M. (2011). Gamma oscillations in the hippocampus require high complex I gene expression and strong functional performance of mitochondria. Brain *134*, 345-358.

Kirchheim, F., Tinnes, S., Haas, C.A., Stegen, M., and Wolfart, J. (2013). Regulation of action potential delays via voltage-gated potassium Kv1.1 channels in dentate granule cells during hippocampal epilepsy. Front Cell Neurosci *7*, 248.
Kumar, H., Kawai, T., Kato, H., Sato, S., Takahashi, K., Coban, C., Yamamoto, M., Uematsu, S., Ishii, K.J., Takeuchi, O., and Akira, S. (2006). Essential role of IPS-1 in innate immune responses against RNA viruses. J Exp Med *203*, 1795-1803.
Lienenklaus, S., Cornitescu, M., Zietara, N., Lyszkiewicz, M., Gekara, N., Jablonska, J., Edenhofer, F., Rajewsky, K., Bruder, D., Hafner, M., *et al.* (2009). Novel reporter mouse reveals constitutive and inflammatory expression of IFN-beta in vivo. J Immunol *183*, 3229-3236.
Madisen, L., Zwingman, T.A., Sunkin, S.M., Oh, S.W., Zariwala, H.A., Gu, H., Ng, L.L., Palmiter, R.D., Hawrylycz, M.J., Jones, A.R., *et al.* (2010). A robust and high-throughput Cre reporting and characterization system for the whole mouse brain. Nat Neurosci *13*, 133-140.
Manahan-Vaughan, D. (1997). Group 1 and 2 metabotropic glutamate receptors play differential roles in hippocampal long-term depression and long-term potentiation in freely moving rats. J Neurosci *17*, 3303-3311.
Morris, R. (1984). Developments of a water-maze procedure for studying spatial learning in the rat. J Neurosci Methods *11*, 47-60.
Osiak, A., Utermohlen, O., Niendorf, S., Horak, I., and Knobeloch, K.P. (2005). ISG15, an interferon-stimulated ubiquitin-like protein, is not essential for STAT1 signaling and responses against vesicular stomatitis and lymphocytic choriomeningitis virus. Mol Cell Biol *25*, 6338-6345.
Porsolt, R.D., Le Pichon, M., and Jalfre, M. (1977). Depression: a new animal model sensitive to antidepressant treatments. Nature *266*, 730-732.
Prinz, M., Schmidt, H., Mildner, A., Knobeloch, K.P., Hanisch, U.K., Raasch, J., Merkler, D., Detje, C., Gutcher, I., Mages, J., *et al.* (2008). Distinct and nonredundant in vivo functions of IFNAR on myeloid cells limit autoimmunity in the central nervous system. Immunity *28*, 675-686.
Ridder, D.A., Lang, M.F., Salinin, S., Roderer, J.P., Struss, M., Maser-Gluth, C., and Schwaninger, M. (2011). TAK1 in brain endothelial cells mediates fever and lethargy. J Exp Med *208*, 2615-2623.
Shannon, P., Markiel, A., Ozier, O., Baliga, N.S., Wang, J.T., Ramage, D., Amin, N., Schwikowski, B., and Ideker, T. (2003). Cytoscape: a software environment for integrated models of biomolecular interaction networks. Genome research *13*, 2498-2504.
Stojdl, D.F., Lichty, B.D., tenOever, B.R., Paterson, J.M., Power, A.T., Knowles, S., Marius, R., Reynard, J., Poliquin, L., Atkins, H., *et al.* (2003). VSV strains with defects in their ability to shutdown innate immunity are potent systemic anti-cancer agents. Cancer Cell *4*, 263-275.
Supek, F., Bosnjak, M., Skunca, N., and Smuc, T. (2011). REVIGO summarizes and visualizes long lists of gene ontology terms. PLoS One *6*, e21800.
Tronche, F., Kellendonk, C., Kretz, O., Gass, P., Anlag, K., Orban, P.C., Bock, R., Klein, R., and Schutz, G. (1999). Disruption of the glucocorticoid receptor gene in the nervous system results in reduced anxiety. Nat Genet *23*, 99-103.
West, M.J., Slomianka, L., and Gundersen, H.J. (1991). Unbiased stereological estimation of the total number of neurons in thesubdivisions of the rat hippocampus using the optical fractionator. The Anatomical record *231*, 482-497.
Zaynagetdinov, R., Sherrill, T.P., Polosukhin, V.V., Han, W., Ausborn, J.A., McLoed, A.G., McMahon, F.B., Gleaves, L.A., Degryse, A.L., Stathopoulos, G.T., *et al.* (2011). A critical role for macrophages in promotion of urethane-induced lung carcinogenesis. J Immunol *187*, 5703-5711.